LBL-32825
UC-401
Preprint

Lawrence Berkeley Laboratory

UNIVERSITY OF CALIFORNIA

CHEMICAL SCIENCES DIVISION

Submitted to Journal of Chemical Physics

High Resolution Photoelectron Spectroscopy and Femtosecond Intramolecular Dynamics of H_2CCO^+ and D_2CCO^+

B. Niu, Y. Bai, and D.A. Shirley

September 1992

LOAN COPY
Circulates
for 4 weeks
Bldg. 50 Library.
LBL-32825
Copy 2

Prepared for the U.S. Department of Energy under Contract Number DE-AC03-76SF00098

DISCLAIMER

This document was prepared as an account of work sponsored by the United States Government. While this document is believed to contain correct information, neither the United States Government nor any agency thereof, nor the Regents of the University of California, nor any of their employees, makes any warranty, express or implied, or assumes any legal responsibility for the accuracy, completeness, or usefulness of any information, apparatus, product, or process disclosed, or represents that its use would not infringe privately owned rights. Reference herein to any specific commercial product, process, or service by its trade name, trademark, manufacturer, or otherwise, does not necessarily constitute or imply its endorsement, recommendation, or favoring by the United States Government or any agency thereof, or the Regents of the University of California. The views and opinions of authors expressed herein do not necessarily state or reflect those of the United States Government or any agency thereof or the Regents of the University of California.

LBL-32825
UC-401

High Resolution Photoelectron Spectroscopy and Femtosecond Intramolecular Dynamics of H_2CCO^+ and D_2CCO^+

Baohua Niu, Ying Bai, and David A. Shirley

Department of Chemistry
University of California

and

Chemical Sciences Division
Lawrence Berkeley Laboratory
University of California
Berkeley, California 94720

September 1992

This work was supported by the Director, Office of Energy Research, Office of Basic Energy Sciences, Chemical Sciences Division, of the U.S. Department of Energy under Contract No. DE-AC03-76SF00098.

High Resolution Photoelectron Spectroscopy and Femtosecond Intramolecular Dynamics of H_2CCO^+ and D_2CCO^+

Baohua Niu, Ying Bai, [1] and David A. Shirley [2]

Department of Chemistry, The University of California at Berkeley

& Chemical Science Division, Lawrence Berkeley Laboratory

One Cyclotron Road, Berkeley, CA 94720, USA.

Abstract

High resolution helium **I**α (584 Å) photoelectron spectra of H_2CCO and D_2CCO are reported. The present spectra of the ground states of ketene cations show more vibrational fine structure than previously reported. The adiabatic ionization energies (**AIEs**) of the cations' first, second and fifth excited states are determined unambiguously. The doublet-like fine structures present in the first excited states of ketene cations imply the excitation of a 'soft' mode that was not observed before. It was assigned to the ν_5 mode, which is characterized by the CH_2 (CD_2) group out-of-plane wagging motion. The complexity of the photoelectron spectra obtained for the ionic first excited states is attributed to the possible dissociation and predissociation of this state. Strong isotope effects are observed in the vibronic (vibrational) couplings in most of the ionic states. Vibrational autocorrelation functions are calculated from the high-resolution photoelectron spectra for four of the six ionic states observed. The dynamics of the ground states of the cations are characterized by a wave packet oscillating with small amplitude around the minimum of the upper potential energy surfaces (**PES**). The decay dynamics of the ionic first and fifth excited states of ketene are characterized by ultrafast intramolecular processes such as dissociation and predissociation.

I. Introduction

The photoelectron spectra of ketene and deuterated ketene have been the subject of extensive experimental and theoretical studies. [1-5] Baker et al. [1] was the first group to obtain the helium **I**α (21.21732 eV) resonance-line photoelectron spectrum of ketene and d_2-ketene. The vibrational fine structures unveiled in this study were partially explained by the then-available theoretical calculations. Hall et al. [4] studied the ketene and d_2-ketene photoelectron spectra using both helium **I**α and helium **II**α (40.81369 eV) resonance lines. The assignments of the adiabatic ionization energies (**AIEs**), the vertical ionization energies (**VIEs**), and some vibrational fine structure analysis were also given. [1-5] The theoretical works have been based largely on these two experimental studies. Very recently, in an ***ab initio*** study of ketene and d_2-ketene, Takeshita [6] has given a detailed theoretical analysis of the photoelectron spectra of ketene and d_2-ketene and of the vibrational fine structures observed in the experimental studies of Baker and Hall. However, the disparity between the experimental and theoretical results is substantial. Especially in the second band (the ionic first excited $\tilde{A}\ 1^2B_2$ state), the sharp onset and the complexity observed in the photoelectron spectrum cannot be reproduced by the theoretical calculation. Hall et al. proposed that the complexity of this band might be due to the predissociation of ketene. Takeshita, on the other hand, showed that ketene cation in the $\tilde{A}$ 1^2B_2 state is stable. He suggested that the complexity might be caused by the superposition of peaks associated with the $\tilde{X}\ 1^2\Pi_g$ band of CO_2^+ and with the second excited $\tilde{B}\ 2^2B_1$ state of ketene. The simplicity of the theoretical band compared with the experimental one was attributed to the near degeneracy of vibrations (**Fermi** resonances), $\nu_2 \approx 2\nu_4$, and $\nu_3 \approx \nu_4$, and might also be attributed to the inadequacy of the theoretical calculation caused by the neglecting of the anharmonicity and the couplings among the vibrations. There were clearly disagreements between the vibrational progression length observed in the experiments and the theoretical calculations. There are extensive studies [45]

of the photochemistry and unimolecular dissociation dynamics of the neutral ketene molecule. The photochemistry and unimolecular dynamics of ketene cations, however, have not attracted much attention so far.

In this work, we report high resolution (FWHM 12 meV) helium Iα photoelectron spectra of H_2CCO and D_2CCO. Improved resolution and effective rotational cooling of the sample by supersonic expansion enabled us to determine the adiabatic ionization potentials (AIEs) for the states accessible by the helium Iα resonance line (21.21732 eV) to a much higher accuracy and to give new interpretations of the vibrational structures observed. The results compared very favorably with the ***ab initio*** calculation by Takeshita, although, there are clearly some disagreements between the theoretically calculated spectra and the experimentally observed ones. Using the autocorrelation function formalism first discussed by Heller [7-10] for electronic photon absorption and emission, developed further later by Lorquet et al. [11-14] and by Ruščić [13] for photoelectron spectroscopy, and modified by Pollard et al. [15] and Reutt et al.; [16,17] the femtosecond ultrafast intramolecular dynamics of the ketene cation in its various ionic states are discussed.

The details of the experiments are described in section **II**. The vibronic coupling and isotope effects on vibronic coupling are discussed briefly in section **III**. A description of, and the method for calculating, the vibrational autocorrelation function are presented in section **IV**. Spectroscopic results and the dynamic interpretations based on the vibrational autocorrelation function are discussed for each of the ionic states of H_2CCO^+ and D_2CCO^+ in section **V**. The major conclusions are summarized in Section **VI**.

II. Experiment

The molecular beam photoelectron spectrometer used for this study has been described in previous publications. [18-20] Briefly, it consists of a supersonic molecular beam source; a windowless helium discharge lamp optimized to produce only the helium

Iα (21.21732 eV) resonance line with minor contamination from higher resonances lines; a quadrupole mass spectrometer (QMS) to characterize the beam composition; a high resolution electron energy analyzer consisting of a 90° spherical sector prefilter and a 180° hemispherical analyzer equipped with a multichannel detector, and associated electron optics; and a dedicated microcomputer (LSI-11/73) for data acquisition and control. The electrons are collected at a 90° angle with respect to the incident photon beam and the supersonic molecular beam and the intensity is uncorrected for angular distribution effects, since there are no ketene ß values for helium Iα photons available.

Approximately 350 torr of ultra high purity helium (99.9999 %, Matheson) was first passed through a U-tube maintained at 77 K to remove trace amounts of water and other impurities in the carrier gas line, then bubbled through a liquid monomer H_2CCO or D_2CCO trap maintained at Hexane/LN_2 slush temperature (177 K) with vapor pressures about 50 torr or 45 Torr as measured with an **MKS** model 122AA-2000 Baratron. The monomer H_2CCO or D_2CCO was prepared following literature procedures [21-23] by thermodecomposition of acetic anhydride and d_6-acetic anhydride(**Aldrich**, 99.5% D-atom) at approximately 823 K, trapping the acetic acid byproduct at 195 K using dry ice/acetone slush and trapping the ketene at 77 K. Ketene or d_2-ketene prepared in this way was vacuum distillated once from 177 K to 77 K to remove trace amounts of acetic acid left and carbon dioxide, the primary byproduct from ketene decomposition. Purified ketene and d_2-ketene were kept in the dark at 77 K with continuous pumping before use.

The He/H_2CCO or He/D_2CCO mixture with a total pressure of approximately 400 Torr was expanded through a 70 μm diameter converging molybdenum nozzle held at room temperature, and skimmed by a 0.858 mm diameter, 6.4 mm tall conical stainless steel skimmer, nozzle-to-skimmer distance = 6.4 mm. The beam source chamber pressure was 6×10^{-5} torr, and the main chamber pressure was 3×10^{-6} torr during the measurements.

All gas inlet lines were minimized and extensively baked (473 K) under vacuum (10^{-7} torr) to remove trace amounts of water and other impurities. Beam compositions were checked by using the **QMS**. No polymers of H_2CCO or D_2CCO, and no CO_2 decomposition byproduct were found in the beam under these experimental conditions. The rotational temperature in the beams was estimated to be ≈ 5 Kelvin as shown by laser induced fluorescence (**LIF**) measurements under similar conditions. [24-26]

The complete photoelectron spectrum of each isotopic species was obtained as five sequential scans of the electron kinetic energy. Each scan was preceded and immediately followed by an argon calibration scan. To enhance statistics, four complete sets of spectra of H_2CCO were scanned and summed. Thus the reported photoelectron bands each represents the summation of four such scans. Individual scans were made within a time period of less than two hours. Restricting the length of each scan limits the total drift in the electron kinetic energy scale to ≤ 1 meV. The linearity of the kinetic energy scale was determined by obtaining the N_2^+ photoelectron spectrum and comparing the N_2^+ $\tilde{X}\,^2\Sigma_g^+$ $v=0$ and $\tilde{B}\,^2\Sigma_u^+$ $v=0$ splitting with the accurate literature value of 3.16981 eV available from N_2^+ optical emission spectroscopy. [27] At higher kinetic energies, the linearity of the energy scale was checked by the photoelectron spectra of argon and xenon. The ionization potentials of these rare gases (I.P. Ar $^2P_{3/2}$ = 15.75975 eV, and Xe $^2P_{3/2}$ = 12.13000 eV) have been precisely determined from optical spectroscopy.[28] The linearity of the molecular beam spectrometer is within ±1.0 meV over this entire energy range. The combination of the drift and the linearity of the energy scale errors limit the accuracy at which the absolute ionization potentials may be reported to ± 3.0 meV. Other spectroscopic constants, however, are obtained as line splittings and may be reported to a much higher accuracy of ± 0.5 meV (4.3 cm^{-1}).

III. Vibronic Coupling and Isotope Effects on Vibronic Coupling

In photoelectron spectroscopy, the vibronic coupling effect, that is the interaction of the electronic and nuclear (vibrational) motion, is often invoked to explain the observations that there are vibrational progressions in modes that are not allowed by the selection rules based on the **Born-Oppenheimer (BO)** approximation; [29] that the observed vibrational frequencies are very low; and that odd quanta of non totally symmetric vibrations get excited. There are other couplings and resonances effects which can also cause similar effects: vibrational-rotation coupling, rotation-electronic couplings and **Fermi** resonances. In general, these effects are much smaller than the vibronic coupling effect and are easier to identify.

Vibronic coupling effects are usually treated as perturbations to the **B O** approximation; that is, the adiabatic Hamiltonian $\mathcal{H}_0$. [30] We can expand the molecular Hamiltonian $\mathcal{H}(q;Q)$, which is a function of the electronic q and the nuclear (normal) Q coordinates, in a Taylor series in the normal coordinates of vibration Q near the equilibrium configuration Q_0:

$$\mathcal{H} = \mathcal{H}(q;Q)_{Q_0} + \sum_{r=1}^{\infty} \left| \frac{1}{r!} \frac{\partial^r \mathcal{H}(q;Q)}{\partial Q^r} \right|_{Q_0} Q^r + \cdots \qquad (1)$$

The first term in equation (1), $\mathcal{H}(q;Q)_{Q_0}$, is called the zeroth-order Hamiltonian, or the **BO** adiabatic Hamiltonian, and is usually expressed as $\mathcal{H}_0$. The coupling of two wave functions Ψ_k and Ψ_j can be expressed according to the matrix elements:

$$\langle \Psi_k | \mathcal{H} | \Psi_j \rangle \qquad (2)$$

which can be expanded with the Hamiltonian $\mathcal{H}$ of equation (1),

$$<\Psi_k|\mathcal{H}|\Psi_j> = <\Psi_k|\mathcal{H}_0|\Psi_j> + \sum_r Q_r \langle\Psi_k\left|\frac{\partial\mathcal{H}}{\partial Q_r}\right|\Psi_j\rangle +$$

$$+\frac{1}{2!}\sum_r Q_r^2 \langle\Psi_k\left|\frac{\partial^2\mathcal{H}}{\partial^2 Q_r^2}\right|\Psi_j\rangle + \frac{1}{2!}\sum_{rs} Q_r Q_s \langle\Psi_k\left|\frac{\partial^2\mathcal{H}}{\partial Q_r \partial Q_s}\right|\Psi_j\rangle + \ldots \quad (3)$$

The first term in equation (3) is always zero by the orthogonality relationship. Thus the necessary conditions for the vibronic coupling effects to perturb the electronic states involved are that at least one term in equation (3) has a nonzero value that it is not too small compared with the zeroth-order electronic states' energy separations.

The total Hamiltonian $\mathcal{H}$ of equation (1) always possesses the full symmetry of the molecular point group and transforms as Γ_1. This is also true for $\mathcal{H}_0$, the Hamiltonian for the zeroth-order unperturbed molecule. For the coupling operators in equation (3): $\partial\mathcal{H}/\partial Q_r$ transforms as the irreducible representation of the normal coordinate Q_r, $\Gamma(Q_r)$; $\partial^2\mathcal{H}/\partial^2 Q_r$ always has at least one component that transforms as Γ_1, the full symmetry of the molecular point group; and $\partial^2\mathcal{H}/\partial Q_r \partial Q_s$ transforms as $\Gamma(Q_r)\otimes\Gamma(Q_s)$. The linear coupling integral in equation (3) will be finite if the product of the representations of all species in the integral contains the totally symmetric representation, Γ_1, that is:

$$\Gamma(\Psi_k)\otimes\Gamma(\Psi_j)\otimes\Gamma(\partial\mathcal{H}/\partial Q_r) \subset \Gamma_1. \quad (4)$$

This will enable the Q_r normal vibrational mode to couple and mix the Ψ_k and Ψ_j electronic states. If Ψ_k and Ψ_j are degenerate states, then Q_r is the asymmetric vibrational mode that will remove the degeneracy. We can discuss the two quadratic terms in equation (3) similarly. The linear terms are usually much larger than the quadratic terms, and the quadratic terms are normally neglected when the linear terms are nonzero. In a polyatomic

molecule, there could be more than one normal mode Q_r that satisfies the condition of equation (4). Those normal modes that satisfy equation (4) are called vibronically active modes. When more than one mode are vibronically active, multimode vibronic coupling effects will occur. In general, these are more complicated to deal with. Multimode vibronic coupling effects and their influence on spectroscopy have been reviewed in detail by Köppel et al. [31]

It can be seen from equation (3) that both the linear and quadratic vibronic couplings depend on the normal coordinates, which are mass-dependent. It is expected that the couplings will be different for isotope-substituted compounds in the same electronic state. One important consequence of this effect is that it is possible for different vibration modes to be excited to a different extent for isotope-substituted compounds. This will cast new difficulties in the interpretation of photoelectron spectra of isotopic compounds. Theoretical calculations have shown that this effect appears in isotope-substituted compounds. [32,33] The H_2CCO^+ and D_2CCO^+ photoelectron spectra have shown this kind of behavior, and they will be discussed further in section V.

IV. The Vibrational Autocorrelation Function

The autocorrelation function formalism description of the intramolecular dynamic process gives complementary information to time-dependent measurements. Lorquet et al.[11-14] first demonstrated how this can be done for photoelectron bands, using the formalism of Heller. [7-10] A variation on the method of Lorquet et al. was used by Pollard et al., [15] and by Reutt et al. [16,17] to study the dynamic characteristics of intramolecular processes using supersonic molecular beam photoelectron spectroscopy. Ruščić [28b] has also given the analytical form of the vibrational autocorrelation function for photoelectron bands under the harmonic approximation for vibrational motions.

Very recently, Remacle et al. [14] have suggested that there exists a relationship between the vibrational autocorrelation function C(t) and the population decay function **P**(t) of a particular electronic state. They defined an average population decay curve $\mathbf{P}_{av}(t)$ valid in a particular time period and $\mathbf{C}_{av}(t)$, the average correlation function, obtained from C(t). It was pointed out by the authors that for a specific excitation, the exact initial rate of decay of $\mathbf{P}_{av}(t)$ (valid up to the dephasing time T_1) is equal to the initial rate of decay of $|C(t)|^2$, and the subsequent time evolution of $\mathbf{P}_{av}(t)$ can be obtained from $|C_{av}(t)|^2$ values that are derived by averaging $|C(t)|^2$ over its oscillation. To a good approximation, the average population decay curve $\mathbf{P}_{av}(t)$ can be obtained by multiplying $|C_{av}(t)|^2$ with an appropriate constant: i.e., the slopes of the two curves are the same.

The autocorrelation function can be expressed as

$$C(t) = |\langle\phi(0)|\phi(t)\rangle|. \tag{5}$$

Here $\phi(0)$ is the initial nuclear wavefunction and $\phi(t)$ is the time evolution of this wavefunction on the excited state potential energy surface (**PES**). C(t) represents the probability amplitude that at time t the system remains in the initially prepared state. It must be noted that the correlation function is the measure of the time evolution of the initial wave packet on the excited-state **PES** and not a measure of the excited state population. But, as mentioned in the preceding paragraph, the initial decay rate of C(t), through $|C(t)|^2$, is the same as the average population $\mathbf{P}_{av}(t)$ initial decay rate. It is dominated by the dephasing of the initial wave packet due to the different shape of the excited-state **PES**. Only at times greater than a vibrational period will radiationless decay processes appear in the correlation function time evolution. The derivation of the autocorrelation function C(t) from photoelectron spectroscopy experimental data has been reported; [12] only the principal

points will be outlined here. The form of photoionization cross section under the strict **Franck-Condon** approximation [34] can be expressed as

$$\sigma(E) \propto \left| |M_{el}(Q,E)|^2 |\langle \Psi'' | \Psi' \rangle|^2 \right| \tag{6}$$

Here $M_{el}(Q, E)$ is the pure electronic transition moment that is a function of the nuclear coordinates Q and electron kinetic energy E, and Ψ'' and Ψ' are the initial- and final-state vibrational wave functions. The electronic transition moment varies slowly over the photoelectron band. In lieu of any arbitrary approximation, a constant value was used in calculating the correlation functions reported here.

Applying the completeness conditions of a set of eigenstates Ψ'' of the molecular Hamiltonian and invoking the analytical form of the Dirac δ function, it has been shown [12] that the cross section for photoionization becomes

$$\sigma(E) \propto \frac{1}{2\pi} \int_{-\infty}^{+\infty} e^{iEt/\hbar} \langle \Psi'' | e^{-i\mathcal{H}t/\hbar} | \Psi'' \rangle \, dt \tag{7}$$

Here $\mathcal{H}$ is the molecular Hamiltonian, Ψ'' is identified as the initial nuclear wave function $\phi(0)$, and $e^{-i\mathcal{H}t/\hbar} |\Psi''\rangle$ is the nuclear wave function at time t: $\phi(t)$. This gives

$$\sigma(E) \propto \frac{1}{2\pi} \int_{-\infty}^{+\infty} e^{iEt/\hbar} \langle \phi(0) | \phi(t) \rangle \, dt \tag{8}$$

and the correlation function can be obtained by a **Fourier** transformation of the cross section

$$C(t) = |\langle \phi(0) | \phi(t) \rangle| \propto \frac{1}{2\pi} \int_{-\infty}^{+\infty} \sigma(E) \, e^{-iEt/\hbar} \, dt \tag{9}$$

This shows that the correlation function can be obtained from the **Fourier** transform of the photoelectron partial cross section $\sigma(E)$. This can be accomplished by deconvoluting the instrument response function $\mathbf{I}(E)_{ir}$, which we determine from the photoelectron spectrum of a rare gas at a kinetic energy comparable to the band of interest, from the quantity $\mathbf{I}(E)$, intensity vs. energy, which we measure in photoelectron spectroscopy. The contributions of the finite rotational temperature in a supersonic molecular beam experiment (typically ~ 5-10 Kelvin) and the rotational excitations contribution to the correlation function were removed by convoluting $\mathbf{I}(E)_{ir}$ with a gaussian function $\mathbf{I}(E)_g$ to generate a rotationally broadened instrument response function. The width of the gaussian function was chosen from the average rotational constant , $\mathbf{B}_{avg}$, of the molecular ion for the particular electronic state (if available), the finite rotational temperature, and the rotational selection rules for photoionization. Ruščić [13] has taken a different approach to account for all the corrections. However, both methods give essentially the same results in the time window of interest.

The procedure for calculating the correlation function of $\tilde{X}$, $\tilde{A}$, $\tilde{B}$, $\tilde{C}$, $\tilde{D}$, and $\tilde{E}$ states of ketene and d_2-ketene cations is the following. First, the band of interest was isolated (in the case of $\tilde{A}$ and $\tilde{B}$ states, they were digitally separated to remove the overlapping of these two bands. The heavy overlapping of the $\tilde{C}$ and $\tilde{D}$ states, however, renders such separation impractical, and was not attempted), and the empirically determined background, plus any constant background was then removed. The resulting band was then normalized (area = 1) and **Fourier** transformed using a discrete **FFT** algorithm. [35] The instrument response function was similarly normalized and convoluted with a Gaussian of 3 meV (FWHM). The resulting function was **Fourier** transformed and divided into that of the data. Finally, the modulus of the previous result was calculated, which gave the correlation function. The procedure can be summarized by the following equation:

$$C^{vib}(t) = |\langle\phi(0)|\phi(t)\rangle| = \left| \int_{-\infty}^{+\infty} I(E)\, e^{-iEt/\hbar}\, dE \right| \div$$

$$\left| \int_{-\infty}^{+\infty} I(E)_{ir}\, e^{-iEt/\hbar}\, dE \;\mathrm{X}\; \int_{-\infty}^{+\infty} I(E)_{g}\, e^{-iEt/\hbar}\, dE \right| \qquad (10)$$

Then $|C(t)|^2$ was then calculated, and $|C_{av}(t)|^2$ was evaluated by fitting $|C(t)|^2$ with an exponential curve of the form Ae^{-ikt} for both the initial drop and the subsequent decay after the first 'vibrational' period.

V. Results and Discussions

The full photoelectron spectra of H_2CCO^+ and D_2CCO^+ obtained by combining four separate scans with a resolution of 12 meV FWHM (as measured with Ar $^2P_{1/2}$, $^2P_{3/2}$) are shown in Figure 1. Table I summarizes the measured spectroscopic constants together with results reported in the literature. [38-40] Each of the six ionic states observed will be discussed separately below.

A. First Band, the $\tilde{X}\ 1^2B_1$ Sate

The ground states of both H_2CCO^+ and D_2CCO^+ showed well-resolved vibrational fine structures, as presented separately in Figure 2. Observed spectroscopic results are presented in Table II. In the present work, effective rotational cooling of the sample by supersonic expansion permits all of the observed vibrational levels to be determined with much improved accuracy, and the mean energies of these transitions were determined by the following least-squares fitting procedure. The adiabatic transitions (or the most intense feature) were first determined by fitting these features to Gaussians. The adiabatic peaks were then isolated and used as empirical functions to fit the successive levels. This

procedure allows the values of the peak splittings to be determined to an accuracy of $\leq \pm$ 0.0005 eV. The mean transition energies located through this procedure are listed for each of the bands observed. The quality of the fit is demonstrated for several vibrational levels of ketene cations in the ground states in Figure 3. The vibrational levels for each normal mode were then least-squares fitted to the standard energy level expression of a Morse oscillator [36,37]

$$G_i^0(V) = \omega_i^0(V) - \omega_i^0 x_i^0(V)^2$$

with the zero point energy being set to zero, ω_i^0 and $\omega_i^0 x_i^0$ are related to ω_i and $\omega_i x_i$ in the following ways: $\omega_i = \omega_i^0 + \omega_i^0 x_i^0$; $\omega_i x_i = \omega_i^0 x_i^0$. Here ω_i is the fundamental vibration frequency, and $\omega_i x_i$ is the quadratic anharmonicity constant for the ith normal vibrational mode.

The result shows that at least two vibrational modes are strongly excited in this state of H_2CCO^+, and for D_2CCO^+ there are additional fine structures in one of the vibrational progressions which is not apparent from the H_2CCO^+ spectrum, indicating that there are more than two modes that are excited strongly. The abnormality in the intensity of the third peak of the $\tilde{X}\ 1^2B_1$ state of H_2CCO^+ and D_2CCO^+ was not explained in the original Baker paper and was not discussed in the study by Hall et al. either. Takeshita attributed this intensity abnormality to the superposition of the two possible vibrational levels, $\nu_2 = 1$ and $\nu_4 = 2$. The present study, however, shows that $\nu_2 \neq 2\nu_4$. Instead, the abnormality of the intensity of this peak was attributed to a **Fermi** resonances, in which one peak "borrows" intensity from its nearby neighbor. Here it is the $\nu_2 = 1$ peak that borrows intensity from the $\nu_4 = 2$ peak. In the case of D_2CCO^+, the situation is similar, but it is the $\nu_3 = 2$ peak that borrows intensity from the $3_0^1 4_0^1$ peak. The weak excitation of the ν_3 mode in H_2CCO^+ was further established by the D_2CCO^+ spectrum, where a reduction in

frequency was apparent for the excitation of the ν_3 mode which accounts for the doublet-like structure in the second, the fourth , the sixth and the eighth peaks in the D_2CCO^+ spectrum. This observation also indicates that the vibronic couplings of the two isotopic molecules in this state are different. This accounts for the stronger excitation of the ν_3 mode in D_2CCO^+ compared with that of H_2CCO^+. In other words, the **PES** of the $\tilde{X}\ 1^2B_1$ state for H_2CCO^+ and D_2CCO^+ are different, especially along the Q_3 normal coordinate in the **Franck-Condon** region. The strong excitation of ν_2, ν_3, and ν_4 modes in the $\tilde{X}$ 1^2B_1 state of H_2CCO^+ and D_2CCO^+ and the intensity of the adiabatic peak indicate that the electron being ejected is mostly from the non-bonding oxygen lone pair.

The vibrational autocorrelation functions calculated from the $\tilde{X}\ 1^2B_1$ state of each ion are shown in Figure 4. Very similar oscillatory patterns are evident for each isotopic species. The beat pattern results from the phase relationship of a stable two-mode anharmonic oscillator system with $\nu_2 \geq 2\nu_3, 2\nu_4$. At shorter times a dephasing of the wave packet, due to the differences in the ionic and neutral potential energy surfaces, dominates the correlation functions. After 10.4 fs for H_2CCO^+ (10.5 fs for D_2CCO^+) the fastest components of the wave packet return to the initial positions on the ionic potential energy surfaces and a reduced maximum of the correlation functions of 0.38 (0.42 for D_2CCO^+) is achieved. This corresponds very closely to one period of ν_2 vibration motion. The slower components of the wave packet, which must also travel along the ν_3, ν_4 coordinates, are expected to return to the initial position on the ionic potential energy surfaces after approximately one period of ν_3/ν_4 vibrational motion. The observed maxima in the correlation functions of 0.78 at 30.5 fs and 0.83 at 30.8 fs for H_2CCO^+ and D_2CCO^+, respectively, are mainly attributed to this return. The small shifts in times of the observed peaks in the correlation functions arise from the spreading of the wave packet on

the anharmonic potential energy surfaces and the relative phase relationships between the ν_2 and ν_3, ν_4 normal modes.

High correlation is maintained at longer times (> 0.3 at 200 fs), which indicates that the initially prepared wave packet is fairly stable regarding deformations along the Q_2 and Q_3/Q_4 normal coordinates. Relatively shallow minima observed in the correlation function are characteristic of a wave packet prepared through a predominately adiabatic transition. The initially prepared wave packet is mostly localized around the minimum of the upper potential energy surfaces along the Q_2 and Q_3/Q_4 normal coordinates, and weakly oscillates around this region, retaining substantially high level correlation at all times.

The isotope effect is also noticeable in the correlation functions, referring to Figure 5, where the correlation functions of the $\tilde{X}\ 1^2B_1$ state of H_2CCO^+ and D_2CCO^+ are plotted together. At shorter times it can be seen that the overall shapes and trends in the correlation function for both isotopic species are almost identical, indicating that the predominant characters of the normal vibration modes involved have very little contribution from the CH_2 or CD_2 groups. At longer times, however, the differences between the correlation functions of the isotopic species are apparent. This can be attributed largely to the differences in the ionic potential energy surfaces between the isotopic species as indicated by the different anharmonicity constants for each normal mode.

B. Second Band, the $\tilde{A}\ 1^2B_2$ State

The second bands of ketene for both isotopic species, which showed well-resolved vibrational fine structures albeit overlapped strongly with the third band $\tilde{B}\ 2^2B_1$ state, are presented in Figure 6, which shows the $\tilde{B}\ 2^2B_1$ states of both isotopic species as well. Observed spectroscopic constants for these states are summarized in Table III. In the present work, effective rotational cooling and the very high resolution achieved unveiled the details of the vibrational progressions in the $\tilde{A}\ 1^2B_2$ state for both isotopic species for

the first time. The vibrational assignments for the $\tilde{A}\ 1^2B_2$ state are well established in the present study based on the ***ab initio*** calculation by Takeshita, except for the possible excitation of another 'soft' mode which causes the doublet-like structures observed in the first few vibrational progressions of this band for both isotopic species. Hall et al. [4] explained the complexity of this band in terms of predissociation of the cation in this state, quoting no detectable emission from this state as an indication for the short life-time implied. Takeshita, however, in an ***ab initio*** calculation, showed that the cation in this state is stable, and the C_{2V} geometry is a true equilibrium configuration. He attributed the complexity of this band to the possible contamination from the $CO_2^+\ \tilde{X}\ ^2\Pi_g$ band near 13.8 eV and the contributions from the $\tilde{B}\ 2^2B_1$ state of ketene above 14.6 eV.

We can first eliminate the possibility of the $CO_2^+\ \tilde{X}\ ^2\Pi_g$ band contamination from the present spectrum of this band. The $CO_2^+\ \tilde{X}\ ^2\Pi_g$ band **AIE** is 13.7778 eV [41], and the 20 meV spin-orbit splitting present in the band would have been evident if there were any contributions from the $CO_2^+\ \tilde{X}\ ^2\Pi_g$ band. Also, experiments performed at 177 K (CO_2 vapor pressure $\leq$ 100 torr) and at 195 K temperature (CO_2 vapor pressure $\geq$ 760 torr) showed no sign of changes in relative intensities for this band. This and the **QMS** diagnosis results established that the ketene sample used for this study had not been contaminated by the dissociation of ketene by-product CO_2. The contributions from the $\tilde{B}\ 2^2B_1$ band of the ketene cation can be rejected, because the very distinct long vibrational progressions observed for the $\tilde{B}\ 2^2B_1$ band in both isotopic species cannot possibly broaden or complicate the vibrational progressions of the $\tilde{A}\ 1^2B_2$ state. We attribute the complexity of this band to the possible predissociation of this band by another close-lying repulsive state or the possible vibrational predissociation of this band above 14.5 eV. The tail of this band extends all the way to the next observed band, the $\tilde{B}\ 2^2B_1$ state. The relatively short vibrational progressions observed in this ($\tilde{A}\ 1^2B_2$) band for both isotopic

species support the predissociation mechanism. The major vibrational progression observed is attributed to the excitations of the ν_2 and ν_4 modes. The apparent insensitivity to isotope substitution of the vibrational progressions implies that the ν_2 and ν_4 modes are predominately C=C=O stretching motions. The differences in the observed vibrational frequencies excluded the validity of the relationships: $\nu_2 \approx 2\nu_4$ and $\nu_3 \approx \nu_4$ shown in the calculated vibrational frequencies by Takeshita. The doublet-like structures observed in the first few vibrational progressions indicate that at least one 'soft' mode has been excited along with the excitation of the ν_2 and ν_4 modes. The large reduction in the splittings among the doublet-like structures upon deuteration (~460.54 cm^{-1} in the $\tilde{A}\ 1^2B_2$ state of H_2CCO^+ vs. ~299.32 cm^{-1} of D_2CCO^+, calculated from the first doublet structure in this band for both isotopic species) implied that this mode might have involved the CH_2 and CD_2 group in the molecular ions. Following the convention of Duncan et al., [38,39] and Allen et al. [42-44] of orienting the molecule on the yz plane, this is most likely the ν_5 mode, which is characterized by the CH_2 (CD_2) group out-of-plane wagging motion, that is excited. Without supporting evidence from other measurements, especially rotationally resolved spectroscopic studies on ketene cations in this state, the assignment of the ν_5 mode could only be regarded as tentative at best. Further theoretical characterization of the **PES** of this state would be extremely helpful in this regard. The strong couplings among vibrational modes revealed by the high-resolution optical studies of Duncan et al. [38,39] on the neutral $\tilde{X}\ ^1A_1$ ground state of ketene showed the complexity of the vibrational modes in ketene. The same or even more complex couplings among vibrational modes can be expected for the ketene cations, as shown in this study for this band.

The vibrational autocorrelation functions, calculated using the formalism and procedure described in section IV for this state in both isotopic species, by digitally removing the $\tilde{B}\ 2^2B_1$ state, are shown in Figure 7. The most striking feature of the correlation functions is the loss of correlation strength on a very short time scale. After

only 6.2 fs in H_2CCO^+ and only 7.5 fs in D_2CCO^+ the correlation functions reached only 0.15 and 0.01, respectively. Thereafter, the correlation functions never regained their initial strengths, and there were no recognizable major oscillations. The ultrafast loss of correlation strength indicates that the initially prepared wave packet was displaced substantially from the minimum of the upper potential energy surfaces. The absence of the return of major oscillations strength implied that the wave packet never got back to its initial position on the upper potential energy surfaces and never regained its initial shape. The calculated $|C_{av}(t)|^2$ were also included in Figure 6. Adopting the method of Remacle et al.,[14] the initial and subsequent drops of the correlation functions ($[C(t)]^2$) were fitted to the exponential forms $A_i \cdot e^{-k_i t}$ and $A_f\, e^{-k_f t}$, respectively, where $A_i = 1.0$ as the initial conditions and k_i were varied and A_f, k_f both were varied in the fits. The total curves were obtained by setting $A_i = 1.0 - A_f$ and $|C_{av}(t)|^2 = A_i \cdot e^{-k_i t} + A_f\, e^{-k_f t}$. We got $k_i = 0.95$ (fs^{-1}) and $k_f = 0.01$ for H_2CCO^+, and $k_i = 0.70$ and $k_f = 0.01$ for D_2CCO^+. This led to the extremely fast population decay rates on the order of 1.1 fs and 1.4 fs for the initial, 100 fs for the subsequent decay of ketene cations. The 100 fs subsequent decay rates could only be regarded as an order of magnitude, since the correlation strengths were very weak in both isotopic species after the initial decay. As discussed by Remacle et al., the initial drops in correlation functions calculated from photoelectron spectra are very sensitive to the 'wings' in the photoelectron spectra. The experimental control of the wings was extremely difficult due to the low signal-to-noise ratio. Thus the calculated initial population-decay rate constants could only be used as indications of the order of magnitude involved. The extremely fast initial decay of the population, as manifested by the correlation function of this state on the order of a few femtosecond, implied upper potential energy surfaces very different from the neutral ground state ones according to the theoretical treatment of Ruščić.[13] The absence of any detectable emissions from this state implied that ultrafast

intramolecular processes are important in the decay of ketene cations from this state. This also supports the argument presented above that ketene cation in the $\tilde{A}\ 1^2B_2$ state might have been predissociated in the **Franck-Condon** region.

C. Third Band, the $\tilde{B}\ 2^2B_1$ State

The third bands of ketene for both isotopic species, with fully resolved vibrational fine structures, are also presented in Fig 6. The observed spectroscopic constants are summarized in Table IV. The adiabatic ionization energies are established by this study to be 14.6089(8)±0.003 and 14.6106(5)±0.003 eV for H_2CCO and D_2CCO, respectively. Takeshita [6] has placed the **AIE** for this band around 14.38 eV, based largely on the **Franck-Condon** factor (**FCF**) calculations. Referring to the H_2CCO^+ spectrum of this band, however, if the **AIE** were lower than 14.609 eV, we would have seen another sharp peak in the spectrum near 14.50 eV that would stand out compared with contributions from the $\tilde{A}\ 1^2B_2$ state. The observed abnormality in intensity in the fifth peak of the H_2CCO^+ spectrum might be attributed to a **Fermi** resonances. In addition to the main vibrational progression, which we assigned as the ν_4 mode, there is another much weaker progression with similar spacing. The splitting between the two progressions observed is 346.7±8cm^{-1} which, as in the $\tilde{A}\ 1^2B_2$ state, might be assigned to another 'soft' mode ν_6, which is characterized as the C=C=O skeleton out-of-plane bending, based largely on the insensitivity of this splitting to deuteration.

For the D_2CCO^+ spectrum, the present high-resolution study revealed more fine structure than observed previously by both Baker et al. and Hall et al.. The additional vibrational progressions present in D_2CCO^+ beyond those present in the H_2CCO^+ spectrum seemed to be the combination of exciting the ν_4 mode with one quantum of the ν_3 mode. This assignment was largely based on the ***ab initio*** calculation of this band by Takeshita,[6] although the calculated spectrum appeared to be much simpler and has much less fine

structure due to the inadequacy inherent in the calculation. The excitation of four vibrational modes in this band makes the definitive assignment of this band extremely difficult especially regarding the assignment of the excitation of ν_6, just as in the H_2COO^+ spectrum of this band. Nonetheless, the present study can be expected to spur theoretical interest to perform high level, multimode calculations to further our understanding on the structure and spectroscopy of ketene cation in the $\tilde{B}\ 2^2B_1$ state in the near future. And again, the differences in vibrational excitations and length of the progressions observed in D_2CCO^+ implied that the ionic **PES** in the **Franck-Condon** region and the vibronic couplings are different for isotopic molecules, as discussed in section III.

The correlation functions calculated for this band for both isotopic species are shown in Figures 8. The fast initial drop in correlation strength and the deep valleys in the correlation functions indicated a substantially different upper **PES** than the neutral ground state one for both isotopic species in the **Franck-Condon** region. The initial position of the wave packet was displaced from the equilibrium geometry, which is consistent with the observed extensive vibrational progressions. The wave packet oscillated with rather large amplitude on the upper **PES**, mostly along the Q_4 normal coordinate. After 35.1 fs for H_2CCO^+ (35.2 fs for D_2CCO^+) the wave packet returned to the initial position on the ionic potential energy surfaces and a reduced maximum of C(t) 0.86 (0.79) was achieved. This corresponded very closely to one period of ν_4 vibrational motion, and the major oscillation in the correlation function for both isotopic species had a period close to the ν_4 normal mode. The ionic **PES** thus is strongly bound along the Q_4 normal coordinate. The slow decaying of the major oscillation of the correlation function was attributed to the spreading of the wave packet due to the anharmonicity of the potential energy surfaces and the weak excitations of other normal modes. The calculated $|C_{av}(t)|^2$ indicated a population decay rate on the order of 100 fs for both isotopic species. The multiplet-like structures in the photoelectron spectrum of D_2CCO^+ of this band, however, induced additional spreading of

the wave packet, which accounts for the loss of correlation to noise level for this band after 74 fs. The stability of this state also supported the assignment of the $\tilde{A}\ 1^2B_2$ state proposed in the preceding section: that the $\tilde{A}\ 1^2B_2$ state might be predissociated. The gradually rising 'background' observed in the $\tilde{B}\ 2^2B_1$ state of the ketene cation spectrum was caused mainly by the overlapping tail of the $\tilde{A}\ 1^2B_2$ state.

D. Fourth and Fifth Bands, the $\tilde{C}\ 2^2B_2$ and the $\tilde{D}\ 1^2A_1$ States

The photoelectron spectra of these two bands, as show in Figure 9, overlapped heavily, and they will be discussed together here. Observed spectroscopic constants are tabulated in Table V for the $\tilde{C}\ 2^2B_2$ state, and in Table VI for the $\tilde{D}\ 1^2A_1$ states. The $\tilde{C}\ 2^2B_2$ states of both isotopic species had well characterized vibrational progressions and are very similar in appearance. The major vibrational progression, upon deuteration, had a significant reduction in frequency and was assigned to the ν_3 mode, supporting the assignment of Hall et al.. [4] Takeshita, [6] however, favored the assignment of this progression to the ν_4 mode. As discussed for the $\tilde{X}\ 1^2B_1$ state, the strong coupling and mixing among different vibrational modes in ketene made the assignment only tentative without rotationally resolved studies. The gradually rising 'background' towards higher IEs of the $\tilde{C}\ 2^2B_2$ state were mostly attributed to the contributions by the overlapping, dissociative $\tilde{D}\ 1^2A_1$ state. The AIE values of the $\tilde{D}\ 1^2A_1$ state listed in Table V can only be regarded as the best estimate in the same spirit, because of the completely dissociative nature of this band in the **Franck-Condon** region. The ***ab initio*** calculation results, however, gave spacing among vibrational progressions on the order of 40 meV for the $\tilde{D}\ 1^2A_1$ state with strong excitation of the ν_4 normal mode along with weak excitations of the ν_1 and ν_3 normal modes. Thus it was rather unexpected that the present high resolution study did not unveil these progressions fully. The qualitative disagreements between the calculated and the experimental spectra for the $\tilde{D}\ 1^2A_1$ state thus indicated that the **PES** of

ketene cations in the **Franck-Condon** region must be very different from the neutral ground state and have a large anharmonicity constant in disagreement with the theoretical calculated spectrum based on harmonic potentials. Further high level calculations, and possible rotationally resolved studies by other spectroscopic means, would be very helpful in solving this difficulty.

The heavy overlapping of these two states precluded any simple means of separating them. No attempt was made to calculate the correlation functions for these two states. However, the overall FWHM of 12.5 meV for most of the peaks observed in the $\tilde{C}$ 2^2B_2 state and the shapes of the peaks indicated that the $\tilde{C}$ 2^2B_2 states were bound in the **Frank-Condon** region. The rather broad and complicated band shapes of the $\tilde{D}$ 1^2A_1 states, on the other hand, indicated that the $\tilde{D}$ 1^2A_1 states might be repulsive over part of the **PES** probed by photoelectron spectroscopy. The full nature of the **PES** for this state awaits further theoretical and experimental investigations.

E. Sixth Band, the $\tilde{E}$ 2^2A_1 State

The photoelectron spectra of this band for both isotopic species are shown in Figures 10. The measured spectroscopic information is summarized in Table VII. Earlier experimental studies of this band had been impeded by the presence of CO_2 impurity and by the possible overlapping from the CO_2^+ $\tilde{B}$ $^2\Sigma_u^+$ state. The present spectrum showed essentially no contamination from the CO_2^+ $\tilde{B}$ $^2\Sigma_u^+$ state as discussed above with the $\tilde{A}$ 1^2B_2 state of ketene and d_2-ketene. Even with the present high resolution achieved and the effective rotational cooling, the width of the adiabatic peak for both isotopic species was much broader than the instrumental resolution and cannot be accounted for by invoking rotational broadening. The width, almost 40 meV **FWHM** for the adiabatic peaks, and the asymmetric shapes of the peaks, as well as the absence of any major vibrational progressions, implied that other intramolecular processes were at play.

The correlation functions calculated for these states are shown in Figures 11 for H_2CCO^+ and D_2CCO^+. The ultrafast loss of correlation strength and the absence of the any major oscillation in the correlation function indicates lifetime broadening. The population decay rates calculated are τ (1/k) equal to: 3 and 4 fs for the initial drop; and 22.2 and 28.5 fs for the late decay for H_2CCO^+ and D_2CCO^+, respectively. These clearly imply that the $\tilde{E}\ 2^2A_1$ states **PES** are highly repulsive in the region reached by the photoionization excitation process. There are no available theoretical calculations on the **PES** of these states. The details of intramolecular dynamics of these states must await further high level theoretical exploration involving multimode vibronic coupling and anharmonic effects.

VI. Conclusions

A high resolution photoelectron spectroscopy study has been performed on supersonic molecular beams of H_2CCO and D_2CCO. The combination of high resolution and effective rotational cooling by supersonic expansion, as well as a least-squares fitting data reduction procedure, have enabled spectroscopic constants of much improved accuracy to be determined for the $\tilde{X}\ 1^2B_1$, $\tilde{A}\ 1^2B_2$, $\tilde{B}\ 2^2B_1$, $\tilde{C}\ 2^2B_2$, and $\tilde{E}\ 2^2A_1$ states. The **AIEs** for all six ionic states accessible by the helium **I**α radiation are reported to a much higher accuracy than previously available. The complex nature and the strong overlap with other bands left the $\tilde{D}\ 1^2A_1$ state much less well characterized. Most of the spectroscopic constants of the ionic states are obtained here for the first time. This should stimulate further theoretical calculations on a high level. The discrepancies in the observed and calculated spectra in the first and second excited states for the ketene cations pointed out the need to improve the theoretical sophistication to match the currently available experimental results. The first excited state presents a interesting challenge.

Vibrational autocorrelation functions were calculated from the photoelectron bands for all but two electronic states of the ketene cations. The ground $\tilde{X}\ 1^2B_1$ state correlation functions displayed oscillatory patterns, which is characteristic of the virtually undisplaced wave packet composed mainly of two oscillators. The wave packet oscillated with small amplitude around the initial position on the ionic **PES** with little spreading, indicated a fairly stable state in the **Franck-Condon** region. In the calculated $\tilde{A}\ 1^2B_2$ state correlation functions, an ultrafast decay of the wave packet was observed. This was attributed largely to the possible predissociating nature of this state near the initially populated **PES**, which awaits further theoretical characterization. The correlation functions of the $\tilde{E}\ 2^2A_1$ state showed ultrafast decay of the initial prepared wave packet on the ionic **PES** on a time scale of a few femtoseconds. This implied that dissociation and ultrafast intramolecular dynamic processes were among the important decay pathways for the initially prepared wave packet around the **Franck-Condon** region on the ionic **PES** for this state.

Acknowledgment:

This work was supported by the Director, Office of Energy Research, Office of Basic Energy Sciences, Chemical Science Division of the U.S. Department of Energy under Contract No. DE-AC03-76SF00098.

---

1. Participating guest, permanent address: Department of Chemistry, Jilin University of Technology, Changchun, Jilin, The people's Republic of China.

2. Present address: The Pennsylvania State University, 114 Kern Graduate Building, University Park, PA 16802, USA.

References:

1. A. D. Baker, and D. W. Turner, **Chem. Comm.**, 480(1969).
2. D. W. Turner, Phil. Trans. R. Soc., London Ser., A7, 268(1970).
3. D. W. Turner, A. D. Baker, and C. R. Brundle, Molecular Photoelectron Spectroscopy, John Wiley & Sons, London (1970) p139.
4. D. Hall, J. P. Maier, and P. Rosmus, Chem. Phys., 373, 24(1977).
5. D. P. Chong, Theoretical Chim. Acta., 181, 50(1978).
6. K. Takeshita, J. Chem. Phys., 96(2), 1199(1992).
7. E. J. Heller, *ibid*, 68, 2066(1978).
8. E. J. Heller, E. B. Stechel, and M. J. Davis, *ibid*, 73(10), 4720(1980).
9. E. J. Heller, Acc. Chem. Res., 14, 368(1981).
10. E. J. Helller, R. Sundberg, and D. Tanner, J. Chem. Phys., 76, 1822(1982).
11. B. Layh-Nihaut, and J. C. Lorquet, *ibid*, 88(9), 5606(1988).
12. A. J. Lorquet, J. C. Lorquet, J. Delwiche, and M. J. Hubin-Franskin, *ibid*, 76(10), 4692(1982).
13. B. Ruščić *ibid*, 85(7), 3776(1986).
14. F. Remacle, M. Desoute-Lecomte, and J. C. Lorquet, *ibid*, 91(7), 4155(1989).

14a. J. C. Lorquet and V. B. Pavloc-Verevkin, *ibid*, 93(1), 520(1990).

15. J. E Pollard, D. J. Trevor, J. E Reutt, Y. T. Lee, and D. A. Shirley, J. Chem. Phys., 81(2), 5302(1984).
16. J. E. Reutt, L. S. Wang, J. E. Pollard, D. J. Trevor, Y. T. Lee, and D. A. Shirley, *ibid*, 84(6), 3022(1986).
17. J. E. Reutt, L. S. Wang, Y. T. Lee, and D. A. Shirley, *ibid*, 85(12), 6928(1986).
18. J. E. Pollard, D. J. Trevor, Y. T. Lee, and D. A. Shirley, Rev. Sci. Instrum., 52, 1837(1981).

19. J. E. Pollard, Ph.D. Thesis, Department of Chemistry, The University of California at Berkeley, 1982.

20. J. E. Reutt, Ph.D. Thesis, Department of Chemistry, The University of California at Berkeley, 1986.

21. Williams and Hurd, J. Org. Chem., **5**, 122(1940).

22. G. J. Fisher, A. F. Maclean, and A. W. Schwizer, J. Org. Chem., 1055(1952).

23. B. I. Sonobe, and R. N. Rosenfeld, JACS., **105**, 7528(1983).

24. H. Bitto, D. R. Guyer, W. F. Polik, and C. B. Moore, Faraday Trans. Dis. Chem. Soc., **81**, 149(1986).

25. I-Chia Chen, W. H. Green, Jr., and C. B. Moore, J. Chem. Phys., **89(1)**, 314(1988).

26. I-Chia Chen, and C. B. Moore, J. Phys. Chem., **94**, 263,269(1990)

27. A. Lufthus, and P. H. Krupenie, J. Phys. Chem. Ref. Data, **6**, 113(1977).

28. C. E. Moore, ed., Atomic Energy Levels, **Vol. I**, (National Bureau of Standards, Washington D. C., 1958).

29. M. Born, and J. R. Oppenheimer, Ann. Phyz. (Lepzig), **84**, 457-487(1927).

30. J. W. Rabalais, **Principles of Ultraviolet Photoelectron Spectroscopy**, John Wiley & Sons, NY (1979).

31. H. Köppel, W. Domcke, and L. S. Cederbaum, Adv. Chem. Phys., **Vol. LVII**, p59-246(1984).

32. L. S. Cederbaum, and W. Domcke, J. Chem. Phys., 64(2), 603(1976).

33. W. Domcke, and L. S. Cederbaum, ibid, 64(2), 612(1976).

34. S. B. O'Neil, and W. P. Reinhardt, ***ibid***, 69, 2126(1978).

35. E. Oran. Brighan, **The Fast Fourier Transform**, (Prentice-Hall, Englewood Cliffs), p164(1974).

36. J. I. Steinfeld, **An Introduction to Modern Molecular Spectroscopy**, 2nd. ed., The MIT Press, Cambridge, MA, p133(1985).

37. G. Herzberg, **Molecular Spectra and Molecular Structures**, **I. Spectra of Diatomic Molecules**, Van Norstrand Reinhold Com., NY, P93(1950).

38. J. L. Duncan, A. M. Ferguson, J. Harpper, and K. H. Tonge, J. Mol. Spectr., **125**, 196-213(1987)

39. J. L. Duncan, A. M. Ferguson, J. Harpper, and K. H. Tonge, ***ibid***, **122**, 72-93(1987).

40. C. B. Moore, and G. Pimentel, J. Chem. Phys., **38(12)**, 2816(1963).

41. L. S. Wang, J. E. Reutt, Y. T. Lee, and D. A. Shirley, J. Elect. Spectr. and Related Phenomena, **47**, 167-186(1988).

42. W. D. Allen, and H. F. Schaeffer III, J. Chem. Phys., **84**, 2212(1986).

43. W. D. Allen, and H. F. Schaeffer III, ***ibid***, **87**, 7076(1987).

44. W. D. Allen, and H. F. Schaeffer III, ***ibid***., **89**, 2329(1988).

45. R. A. Marcus, Science, **Vol. 256**, p1523, 12 June1992.

46. E. R. Lovejoy, S. K. Kim, and C. B. Moore, **ibid**, **Vol. 256**, p1541(1992).

Table I. Ionization Potentials & Vibrational Frequencies (cm^{-1}) Observed

Ionic States	AIE[a] (eV)	ν_1, $\omega_e x_e$	ν_2, $\omega_e x_e$	ν_3, $\omega_e x_e$	ν_4, $\omega_e x_e$	ν_5, $\omega_e x_e$	ν_6, $\omega_e x_e$
H_2CCO[b] $\tilde{X}\ ^1A_1$		3070.4	2152.6	1387.5	1116.0	587.4	528.4
H_2CCO^+ $\tilde{X}\ 1^2B_2$	9.6191(4)		2263.4 (4.3), 17.4 (4.3)	1378.6 (4.3)	1226.9 (4.3), 99.8 (4.3)		
$\tilde{A}\ 1^2B_2$	13.7967(3)		1527.9 (4.3), -61.7 (4.3)		1164.2 (4.3), 21.1 (4.3)	460.7 (4.3)	689.8(4.3)
$\tilde{B}\ 2^2B_1$	14.6089(8)		2001.2 (4.3), 15.8 (4.3)		1000.8 (4.3), 4.8 (4.3)		346.7 (4.3)
$\tilde{C}\ 2^2B_2$	16.0687(8)		1697.1 (4.3), -1.4 (4.3)	1086.6 (4.3), 7.8 (4.3)			
$\tilde{D}\ 1^2A_1$	16.2393(3)[c]		1488.0 (4.3), -19.5 (4.3)	1164.3 (4.3), 11.5 (4.3)	708.9 (4.3), 4.5 (4.3)		
$\tilde{E}\ 2^2A_1$	18.0897(10)			1177.4 (4.3), 15.0 (4.3)	670.6 (4.3), -4.3 (4.3)		396.9 (4.3), -23.9 (4.3)

TABLE I. Continued

Ionic States	AIE[a] (eV)	ν_1, $\omega_e x_e$	ν_2, $\omega_e x_e$	ν_3, $\omega_e x_e$	ν_4, $\omega_e x_e$	ν_5, $\omega_e x_e$	ν_6, $\omega_e x_e$
D_2CCO[b] $\tilde{X}\,^1A_1$		2267.3	2120.5	1225.1	924.7	541.2	434.7
D_2CCO^+ $\tilde{X}\,1^2B_2$	9.6130(3)		2285.6 (4.3), 20.8 (4.3)	1090.9 (4.3), -6.9 (4.3)	924.7 (4.3), -82.2 (4.3)		
$\tilde{A}\,1^2B_2$	13.8366(8)		2140.4 (4.3), 5.2 (4.3)		1006.6 (4.3), -12.8 (4.3)	299.3 (4.3)	105.8 (4.3)
$\tilde{B}\,2^2B_1$	14.4942(7)		1732.3 (4.3)	848.4 (4.3)	1056.1 (4.3), 0.5 (4.3)		
$\tilde{C}\,2^2B_2$	16.0856(1)		1101.7 (4.3)	799.8 (4.3), 2.1 (4.3)			
$\tilde{D}\,1^2A_1$	16.3204(2)[c]	1266.7 (4.3)	1204.0 (4.3), 8.2 (4.3)	1168.8 (4.3), 13.6 (4.3)			
$\tilde{E}\,2^2A_1$	18.0734(10)	1133.3 (4.3), 12.4 (4.3)	834.4 (4.3)				

(a) The absolute AIEs are accurate to ± 3meV as discussed in the main text. Other spectroscopic constants, however, are obtained as line splittings, and can thus be reported to a much higher accuracy, ±0.5 meV (±4.3 cm^{-1}). (b) From ref. 38-40. (c) Best estimate only. (d) From the splitting in the first two peaks of the $\tilde{A}\,1^2B_2$ state. Numbers in parenthese indicate the uncertanties in the last digit.

TABLE II. Vibrational Levels of the $\tilde{X}\ 1^2B_1$ State

IE[a] H_2CCO^+ (eV)	$(\nu_2\nu_3\nu_4)$	IE[a] D_2CCO^+ (eV)	$(\nu_2\nu_3\nu_4)$
9.6191(4)	000	9.6130(3)	000
9.8954(5)	100	9.8902(9)	100
10.1674(5)	200	10.1628(6)	200
10.4351(3)	300	10.4336(4)	300
9.7465(1)	001	10.6937(2)	400
10.0206(6)	101	9.7478(4)	010
10.2948(1)	201	10.0239(2)	110
10.5646(5)	301	10.3050(5)	210
9.7900(7)	010	10.5634(6)	310
10.0672(5)	110	10.8309(7)	410
10.3135(4)	120	9.7272(4)	001
9.84913(2)	002	10.0030(3)	101
10.1277(3)	102	10.2801(5)	201
10.3959(9)	202	10.5439(2)	301
		10.8063(6)	401
		9.8848(1)	020
		10.1592(4)	120
		10.4295(7)	220
		10.6793(4)	320
		9.8622(8)	002
		10.1408(2)	102
		10.4152(5)	202
		10.6835(7)	302

TABLE II. Continued

ν_2 = 2263.4(4.3), $\omega_e x_e$ = 17.4(4.3)cm^{-1}	ν_2 = 2285.6(4.3), $\omega_e x_e$ = 20.8(4.3)cm^{-1}
ν_3 = 1378.6(4.3), $\omega_e x_e$ = ? cm^{-1}	ν_3 = 1090.9(4.3), $\omega_e x_e$ = -6.9(4.3)cm^{-1}
ν_4 = 1226.9(4.3), $\omega_e x_e$ = 99.8(4.3)cm^{-1}	ν_4 = 924.7 (4.3), $\omega_e x_e$ = -82.2(4.3)cm^{-1}

(a). See footnote in TABLE I.

TABLE III. Vibrational Levels of the $\tilde{A}\ 1^2B_2$ State

IE[a] H_2CCO^+ (eV)	$\nu_2\nu_4\nu_5$	IE[a] D_2CCO^+ (eV)	$\nu_2\nu_4\nu_5$
13.7967(3)	000	13.8366(8)	000
13.9829(2)	100	13.9653(2)	010
14.1925(4)	200	14.0939(7)	020
14.4093(4)	300	14.2337(4)	030
13.9349(5)	010	14.3648(9)	040
14.0694(2)	020	14.5092(8)	050
14.1988(3)	030	13.8737(9)	001
14.3213(4)	040	14.1385(2)	101
13.8538(5)	001	14.4019(7)	201
14.0700(3)	101	13.9331(6)	$000(6_0^1)$
14.2805(5)	201	14.0605(7)	$010(6_0^1)$
14.4846(9)	301	14.1879(7)	$020(6_0^1)$
13.8822(5)	$000(6_0^1)$	14.3188(3)	$030(6_0^1)$
14.0137(2)	$010(6_0^1)$	14.0049(1)	$001(6_0^1)$
14.1347(7)	$020(6_0^1)$	14.2337(4)	$101(6_0^1)$
14.2627(7)	$030(6_0^1)$	14.4625(8)	$201(6_0^1)$
ν_2 = 1527.9(4.3), $\omega_e x_e$ = -61.7(4.3)cm^{-1}		ν_2 = 2140.4 (4.3), $\omega_e x_e$ = 5.2 (4.3)cm^{-1}	
ν_4 = 1164.2 (4.3), $\omega_e x_e$ = 21.1 (4.3)cm^{-1}		ν_4 = 1006.7(4.3), $\omega_e x_e$ = -12.8(4.3)cm^{-1}	
ν_5 = 460.7 (4.3), $\omega_e x_e$ = ? cm^{-1}		ν_5 = 299.3 (4.3) cm^{-1}, $\omega_e x_e$ = ?	
ν_6 = 689.8 (4.3),$\omega_e x_e$ = ? cm^{-1}		ν_6 = 105.8(4.3), $\omega_e x_e$ = ?	

(a). See footnote in TABLE I.

TABLE IV. Vibrational Levels of the $\tilde{B}\ 2^2B_1$ State

IE[a] H_2CCO^+(eV)	$\nu_2\nu_4\nu_6$	IE[a] D_2CCO^+(eV)	$\nu_2\nu_4\nu_6$
14.6089(8)	000	14.6106(5)	000
14.7320(6)	010	14.7404(6)	001
14.8531(9)	(100)[b], 020	14.8725(1)	002
14.9743(2)	030	15.0023(2)	003
15.0934(9)	(200)[b], 040	15.1327(7)	004
15.2107(1)	050	14.7158(4)	010
15.3259(8)	060	14.8478(9)	011
15.44191(1)	070	14.9732(3)	012
15.5662(9)	080	15.1052(8)	013
15.6721(4)	090	15.2328(5)	014
15.7820(9)	0(10)0	15.3787(2)	015
14.6519(6)	001	15.5169(7)	016
14.7672(3)	011	14.8255(1)	100
14.8942(2)	021	14.9530(8)	101
15.0114(4)	031	15.0784(2)	102
15.1403(8)	041	15.2059(9)	103
15.2572(8)	051	15.3358(0)	104
15.3670(1)	061	15.4708(9)	105
15.4805(1)	071	15.0653(6)	110
15.5897(3)	081	15.1836(1)	111
15.7004(1)	091	15.3089(5)	112
15.8072(2)	0(10)1	15.4298(0)	113
		15.5444(0)	114

TABLE IV. Continued

	15.6625(7)	115
	15.7767(1)	116
	15.8841(4)	117
ν_2 = 2001.2(4.3), $\omega_e x_e$ = 15.8(4.3)cm^{-1}	ν_2 = 1732.3(4.3), $\omega_e x_e$ = cm^{-1}	
ν_4 = 1000.8(4.3), $\omega_e x_e$ = 4.8(4.3)cm^{-1}	ν_3 = 848.4 (4.3), $\omega_e x_e$ = cm^{-1}	
ν_6 = 346.7(4.3), $\omega_e x_e$ = cm^{-1}	ν_4 = 1056.1 (4.3), $\omega_e x_e$ = 0.5 (4.3)cm^{-1}	

(a) See footnote in TABLE I. (b) **Fermi** resonances peaks.

TABLE V. Vibrational Levels of the $\tilde{C}\ 2^2B_2$ State

IE[a] H_2CCO^+(eV)	$\nu_2\nu_3$	IE[a] D_2CCO^+(eV)	$\nu_2\nu_3$
16.0687(8)	00	16.0856(1)	00
16.1981(6)	01	16.1889(6)	01
16.3257(5)	02	16.2841(8)	02
16.4567(8)	03	16.3828(3)	03
16.5862(2)	04	16.4761(6)	04
16.7155(5)	05	16.5746(9)	05
16.8365(8)	06	16.6744(1)	06
16.9512(9)	07	16.7666(4)	07
17.0746(8)	08	16.2222(0)	10
16.06878)	00	16.3271(8)	11
16.2790(2)	10	16.4326(9)	12
16.4915(5)	20	16.5323(1)	13
16.7021(8)	30	16.6320(3)	14
16.9121(4)	40		
17.1280(4)	50		
17.3381(9)	60		
16.1721(2)	01		
16.3625(6)	11		
16.5557(4)	21		
16.7443(1)	31		
16.9376(7)	41		
ν_2 = 1697.1(4.3), $\omega_e x_e$ = -1.4 (4.3)cm^{-1}		ν_2 = 1101.7 (4.3) $\omega_e x_e$ = ? cm^{-1}	
ν_3 = 1086.6(4.3), $\omega_e x_e$ = 7.8 (4.3)cm^{-1}		ν_3 = 799.8 (4.3), $\omega_e x_e$ = 2.1 (4.3) cm^{-1}	

(a). See footnote in TABLE I.

TABLE VI. Vibrational Levels of the $\tilde{D}\ 1^2A_1$ State

IE[a] H_2CCO^+(eV)	$\nu_2\nu_3\nu_4$	IE[a] D_2CCO^+(eV)	$\nu_1\nu_2\nu_3$
16.2393(3)	000	16.3204(2)	000
16.4438(5)	100	16.4625(1)	001
16.6267(3)	200	16.5971(3)	002
16.8235(4)	300	16.7367(3)	003
17.0279(0)	400	16.8663(6)	004
17.2422(6)	500	16.9934(9)	005
16.4281(1)	100	16.4774(7)	100
16.5067(7)	101	16.6295(4)	110
16.5913(4)	102	16.7766(1)	120
16.6798(3)	103	16.9162(1)	130
16.7624(2)	104	17.0508(3)	140
16.8450(2)	105	17.1954(1)	150
16.9295(8)	106	17.3399(9)	160
17.0121(8)	107	17.4671(3)	170
17.0869(0)	108		
17.1596(6)	109		
16.5008(8)	101		
16.6346(0)	111		
16.7781(5)	121		
16.9118(8)	131		
17.0495(4)	141		
17.1793(3)	151		
17.3012(5)	161		

TABLE VI. Continued

ν_2 = 1488.0(4.3), $\omega_e x_e$ = -19.5 (4.3)cm^{-1}	ν_1 = 1266.7 (4.3), $\omega_e x_e$ = ? cm^{-1}
ν_3 = 1164.3 (4.3), $\omega_e x_e$ = 11.5(4.3) cm^{-1}	ν_2 = 1204.9 (4.3), $\omega_e x_e$ = 8.2(4.3) cm^{-1}
ν_4 = 708.9 (4.3), $\omega_e x_e$ = 4.5 (4.3) cm^{-1}	ν_3 = 1168.8 (4.3), $\omega_e x_e$ = 13.6(4.3) cm^{-1}

a. See footnote in TABLE I.

TABLE VII. Vibrational Levels of the $\tilde{E}\ 2^2A_1$ State

IE[a] H_2CCO^+(eV)	$\nu_3\nu_4\nu_6$	IE[a] D_2CCO^+(eV)	$\nu_1\nu_2$
18.0897(3)[b]	000	18.0734(5)[b]	00
18.2333(5)	100	18.2101(4)	10
18.3697(4)	200	18.3456(1)	20
18.5061(5)	300	18.4761(5)	30
18.6367(5)	400	18.1768(9)	01
18.1739(5)	010	18.3197(5)	11
18.2593(5)	020	18.4564(5)	21
18.3492(2)	030		
18.4281(7)	040		
18.5234(8)	050		
18.1428(2)	001		
18.2069(9)	002		
18.2719(5)	003		
18.1739(5)	010		
18.3158(6)	110		
18.4465(1)	210		
18.5920(5)	310		
ν_3 = 1177.4 (4.3), $\omega_e x_e$ = 15.0 (4.3)cm^{-1}		ν_1 = 1133.3 (4.3), $\omega_e x_e$ = 12.4(4.3) cm^{-1}	
ν_4 = 670.6 (4.3), $\omega_e x_e$ = -4.3(4.3) cm^{-1}		ν_2 = 834.3 (4.3), $\omega_e x_e$ = ? cm^{-1}	
ν_6[c] = 396.9(4.3), $\omega_e x_e$ = -23.9(4.3) cm^{-1}			

(a) See Table I. footnote. (b) This is only the best estimate ± 10 meV. (c) Tentative values.

Figure Captions:

Figure 1. The full spectrum of ketene and deuterated ketene with a resolution of 12 meV **FWHM**. The designation of the ionic states assumes that the ions have C_{2V} symmetry.

Figure 2. The photoelectron spectrum of the $\tilde{X}\ 1^2B_1$ state of ketene and d_2-ketene, with a resolution of 12 meV FWHM. The vibrational progressions are labeled according to the C_{2V} geometry and 2_0^n stands for the transition

$$M^+ (\nu_2 = n) + e \leftarrow M (\nu_2 = 0) + \hbar\omega$$

following standard spectroscopic notations.

Figure 3. A portion of the $\tilde{X}\ 1^2B_1$ state of H_2CCO (top) and D_2CCO (bottom) are shown together with the results of a least-squares fit to a sum of empirically determined instrument response functions (a Voigt function which is the convolution of a Gaussian function with a Lorentzian function). For details of the assigned vibronic levels, see Figure 2.

Figure 4 The vibrational autocorrelation function of the $\tilde{X}\ 1^2B_1$ state of ketene and d_2-ketene after all corrections have been made. The beat pattern results from the phase relationship of a stable two-mode anharmonic oscillator system, with $\nu_2 \geq 2\nu_3, 2\nu_4$.

Figure 5. The vibrational autocorrelation functions of the $\tilde{X}\ 1^2B_1$ states of ketene and d_2-ketene. The solid line is for ketene and the dotted line is for d_2-ketene. Note the isotope effect at longer times.

Figure 6. The photoelectron spectrum of the $\tilde{A}\ 1^2B_2$ and $\tilde{B}\ 2^2B_1$ states of ketene and d_2-ketene. Note vibrational progressions in the $\tilde{A}\ 1^2B_2$ state were fully

resolved for the first time. Notations are the same as in Figure 2.

Figure 7. The vibrational correlation function calculated for the $\tilde{A}\ 1^2B_2$ state of ketene and d_2-ketene after digitally removing the contributions from the $\tilde{B}\ 2^2B_1$ state, and making all corrections. The most striking feature of the correlation function is the loss of correlation strength on an ultrafast time scale of a few fs. This implies that ketene cations were prepared on the repulsive side of the upper potential energy surface, and were subject to predissociation and other ultrafast intramolecular dynamic processes.

Figure 8. The vibrational correlation function calculated for the $\tilde{B}\ 2^2B_1$ state of ketene and d2-ketene, after digitally removing the contributions from the $\tilde{A}\ 1^2B_2$ state, and making all corrections. The deep valleys in the correlation function indicate a displaced wave packet from the upper potential energy surface (**PES**) minimum.

Figure 9. The photoelectron spectrum of the $\tilde{C}\ 2^2B_2$ and $\tilde{D}\ 1^2A_1$ states of ketene. The major vibrational progression was attributed to the $\tilde{C}\ 2^2B_2$state.

Figure 10. The photoelectron spectrum of the $\tilde{E}\ 2^2A_1$ state of ketene and d_2-ketene. The very broad adiabatic peak and the asymmetric line shape imply that ketene cations in the **Franck-Condon** part of the **PES** are subject to l lifetime broadening effects.

Figure 11. The vibrational correlation function calculated for the $\tilde{E}\ 2^2A_1$ state of ketene and d_2-ketene after all corrections were made. The ultrafast decay of the correlation functions imply that ultra fast intramolecular processes dominate the decay of the ketene cations in the **Franck-Condon** part of the **PES**.

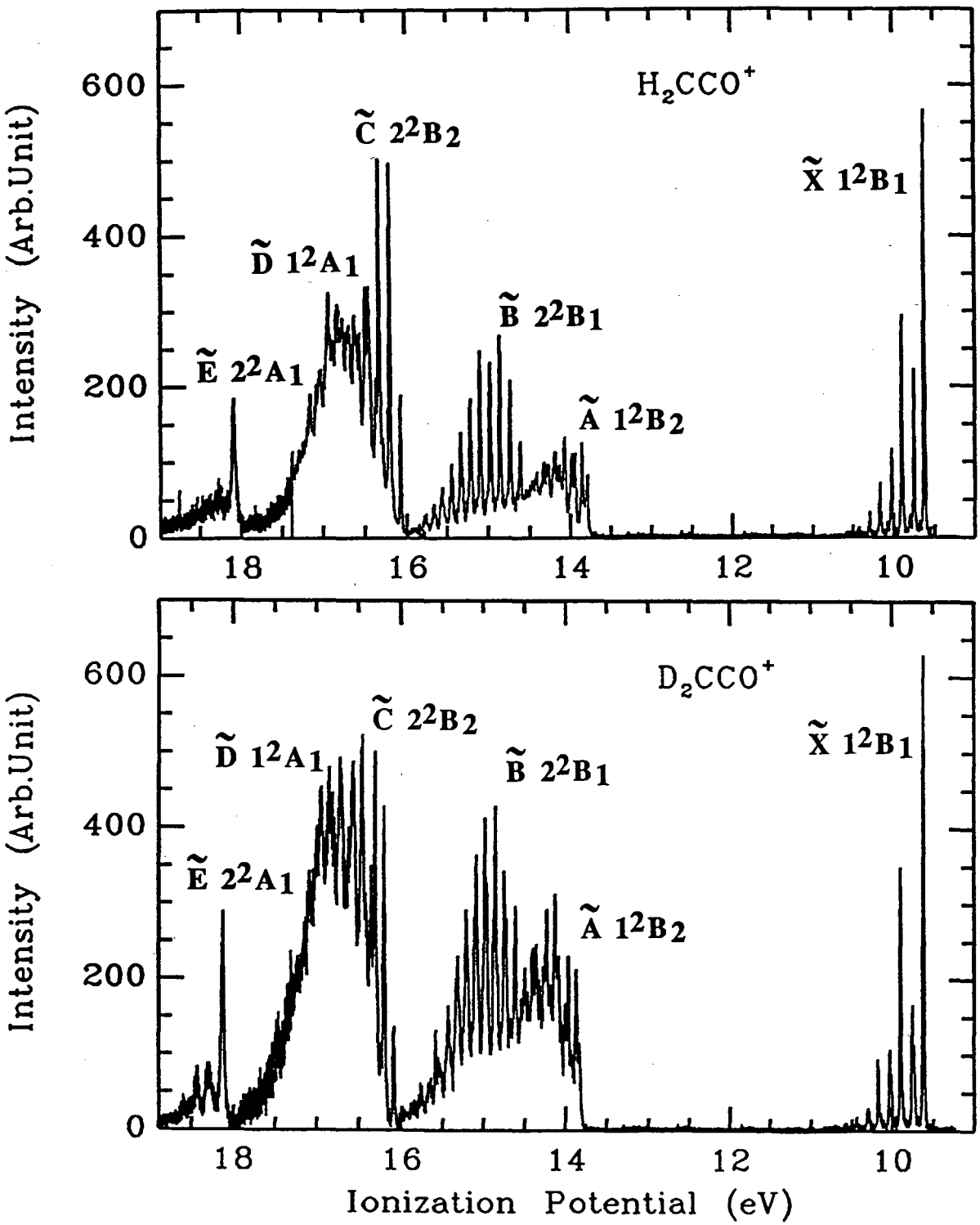
H2CCO+
C̃ 22B2
X̃ 12B1
D̃ 12A1
B̃ 22B1
Ẽ 22A1
Ã 12B2
Intensity (Arb.Unit)
600
400
200
0
18
16
14
12
10
D2CCO+
C̃ 22B2
X̃ 12B1
D̃ 12A1
B̃ 22B1
Ẽ 22A1
Ã 12B2
Intensity (Arb.Unit)
600
400
200
0
18
16
14
12
10
Ionization Potential (eV)

Figure 1

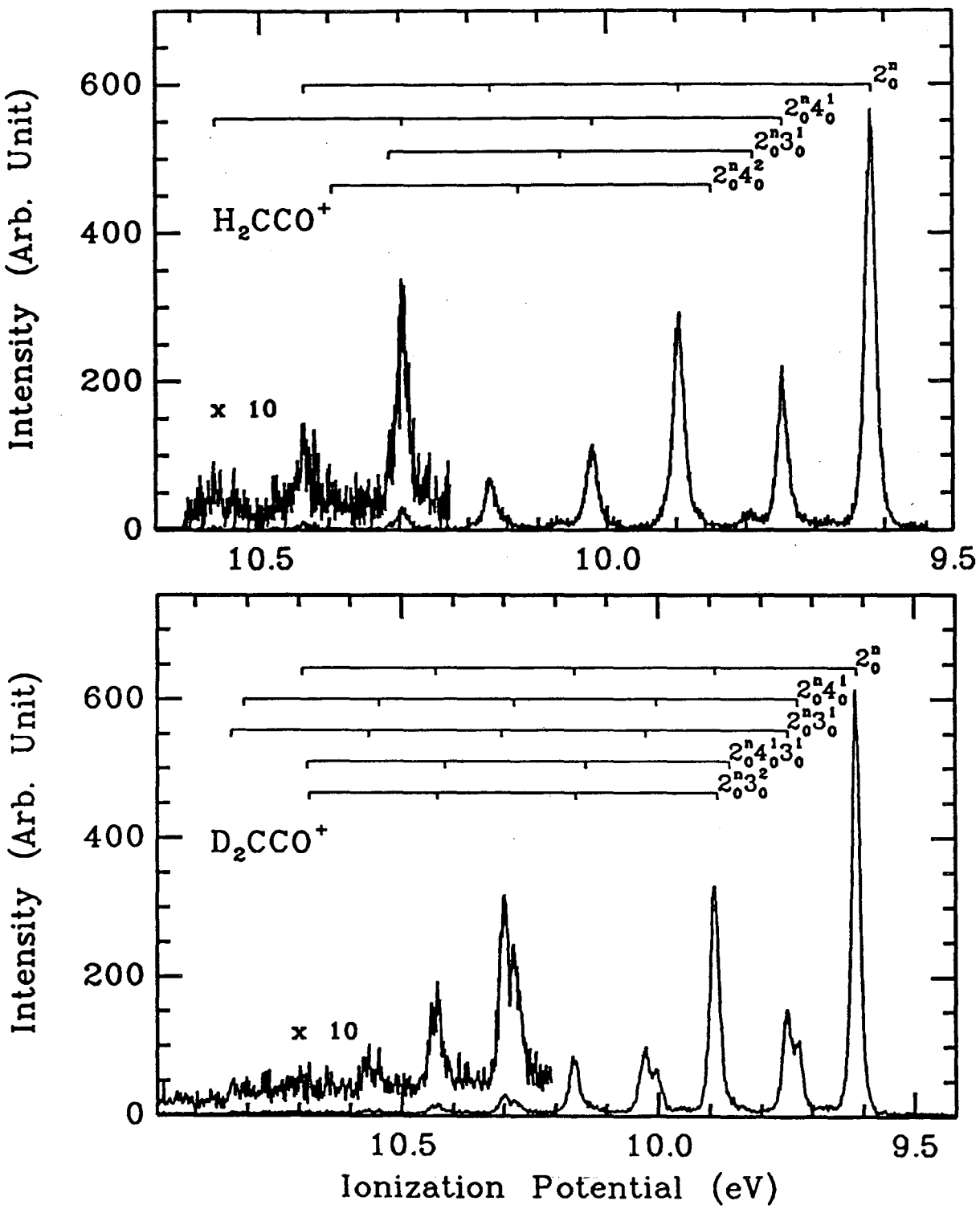
600
400
200
0
Intensity (Arb. Unit)
H_2CCO^+
x 10
2_0^n
$2_0^n4_0^1$
$2_0^n3_0^1$
$2_0^n4_0^2$
10.5
10.0
9.5
600
400
200
0
Intensity (Arb. Unit)
D_2CCO^+
x 10
2_0^n
$2_0^n4_0^1$
$2_0^n3_0^1$
$2_0^n4_0^13_0^1$
$2_0^n3_0^2$
10.5
10.0
9.5
Ionization Potential (eV)

Figure 2

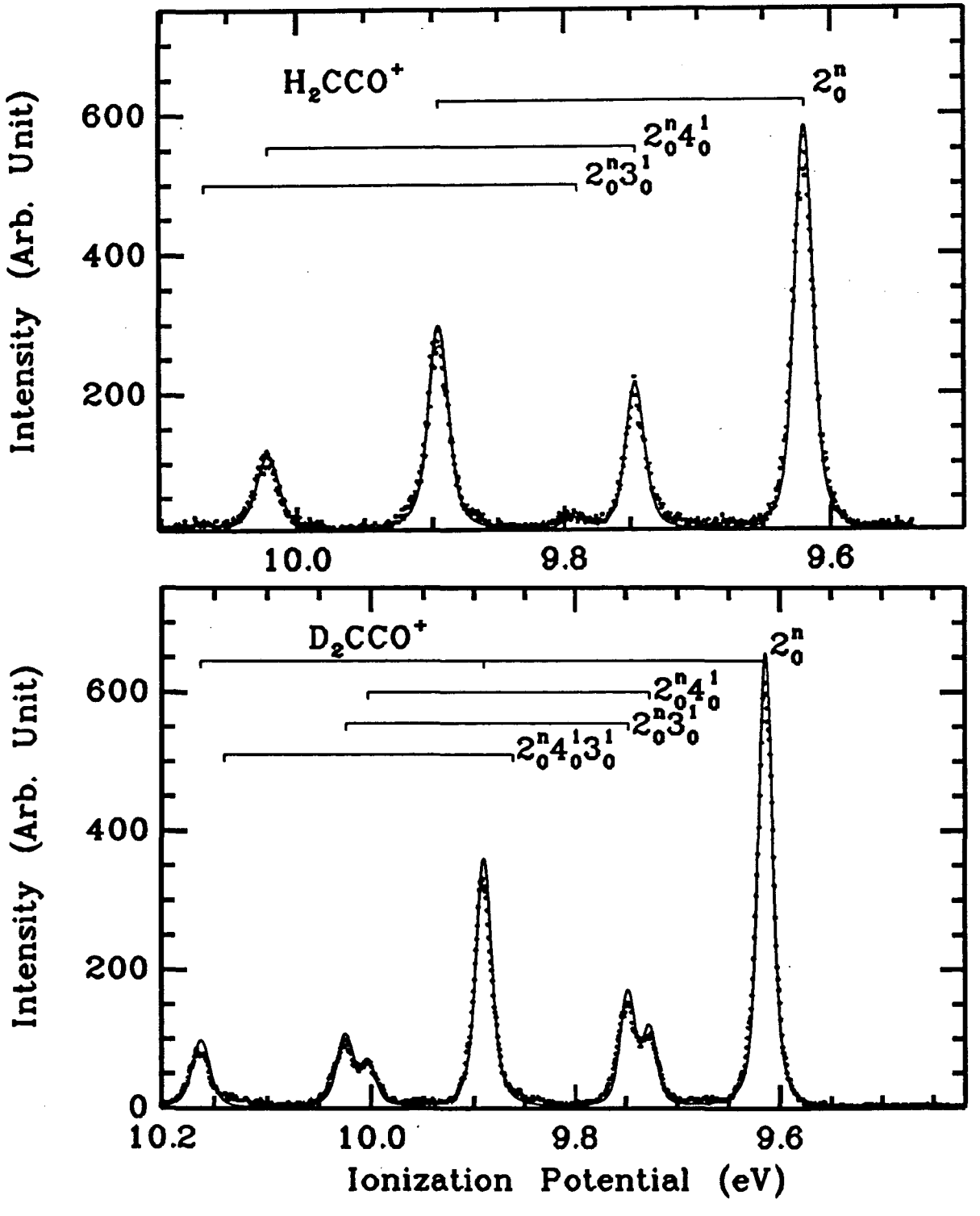
H2CCO+
2n0
2n0 4 1 0
2n0 3 1 0
600
400
200
Intensity (Arb. Unit)
10.0
9.8
9.6
D2CCO+
2n0
2n0 4 1 0
2n0 3 1 0
2n0 4 1 0 3 1 0
600
400
200
0
Intensity (Arb. Unit)
10.2
10.0
9.8
9.6
Ionization Potential (eV)

Figure 3

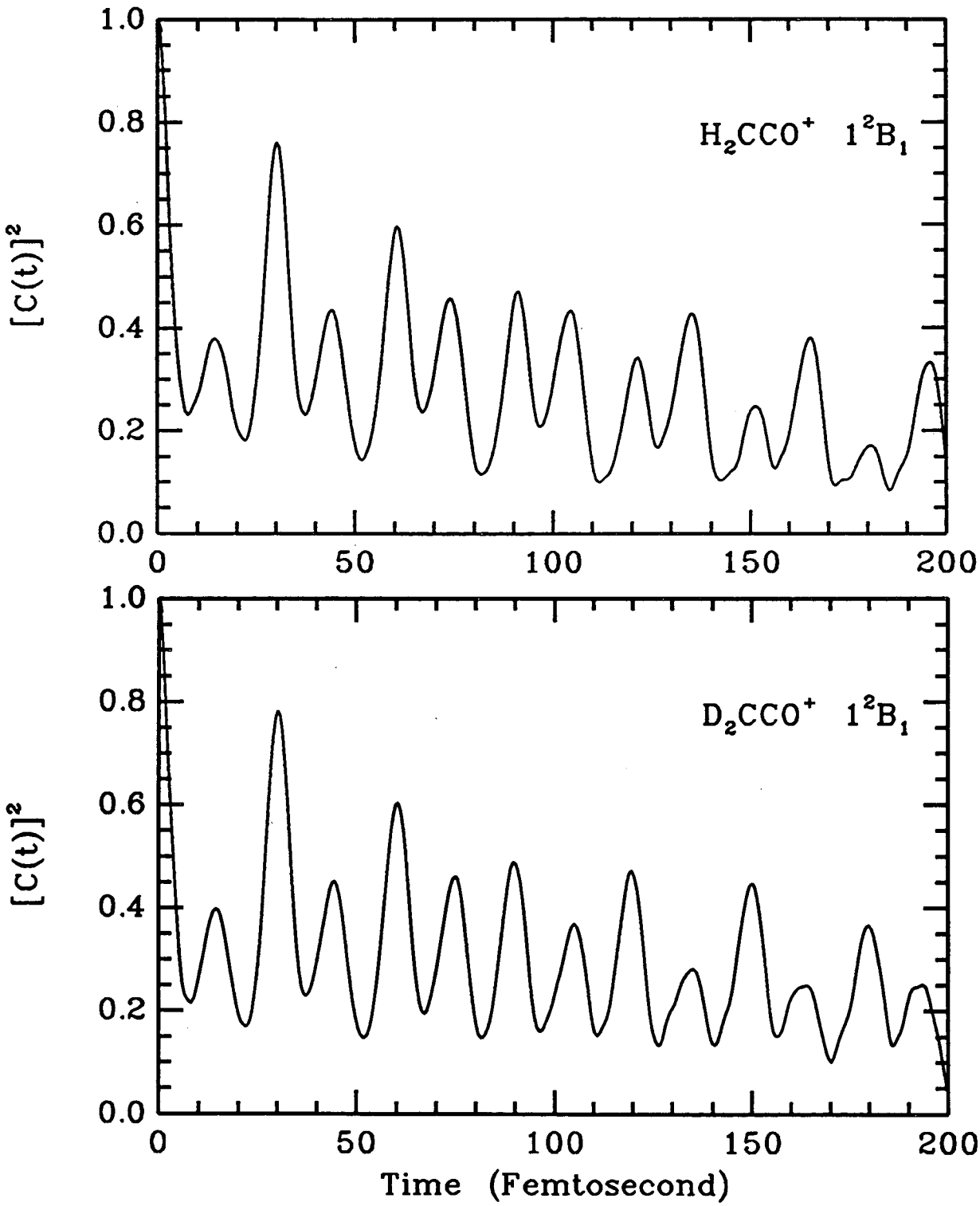
1.0
0.8
0.6
0.4
0.2
0.0
[C(t)]²
H₂CCO⁺ 1²B₁
0
50
100
150
200
D₂CCO⁺ 1²B₁
Time (Femtosecond)

Figure 4

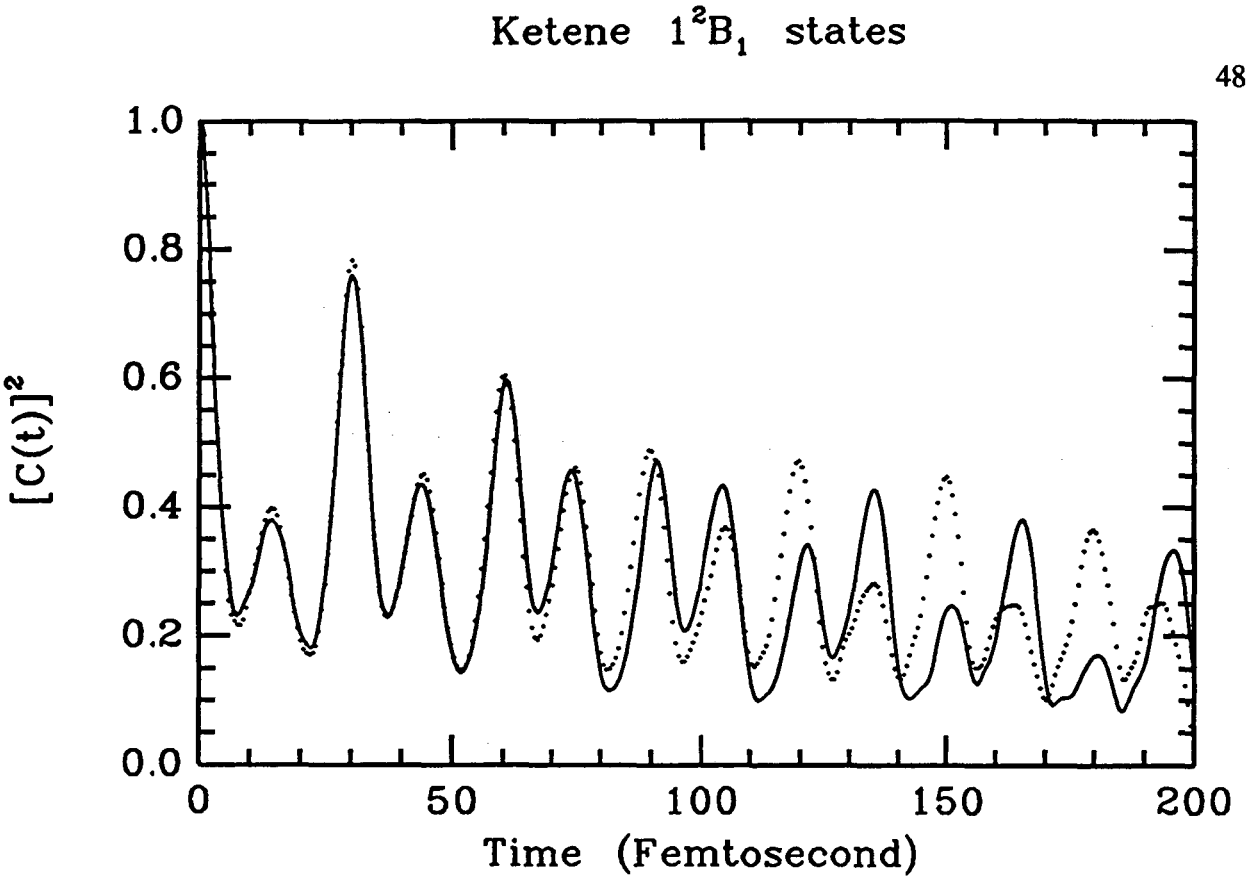
Ketene 1^2B_1 states
1.0
0.8
0.6
0.4
0.2
0.0
$[C(t)]^2$
0
50
100
150
200
Time (Femtosecond)

Figure 5

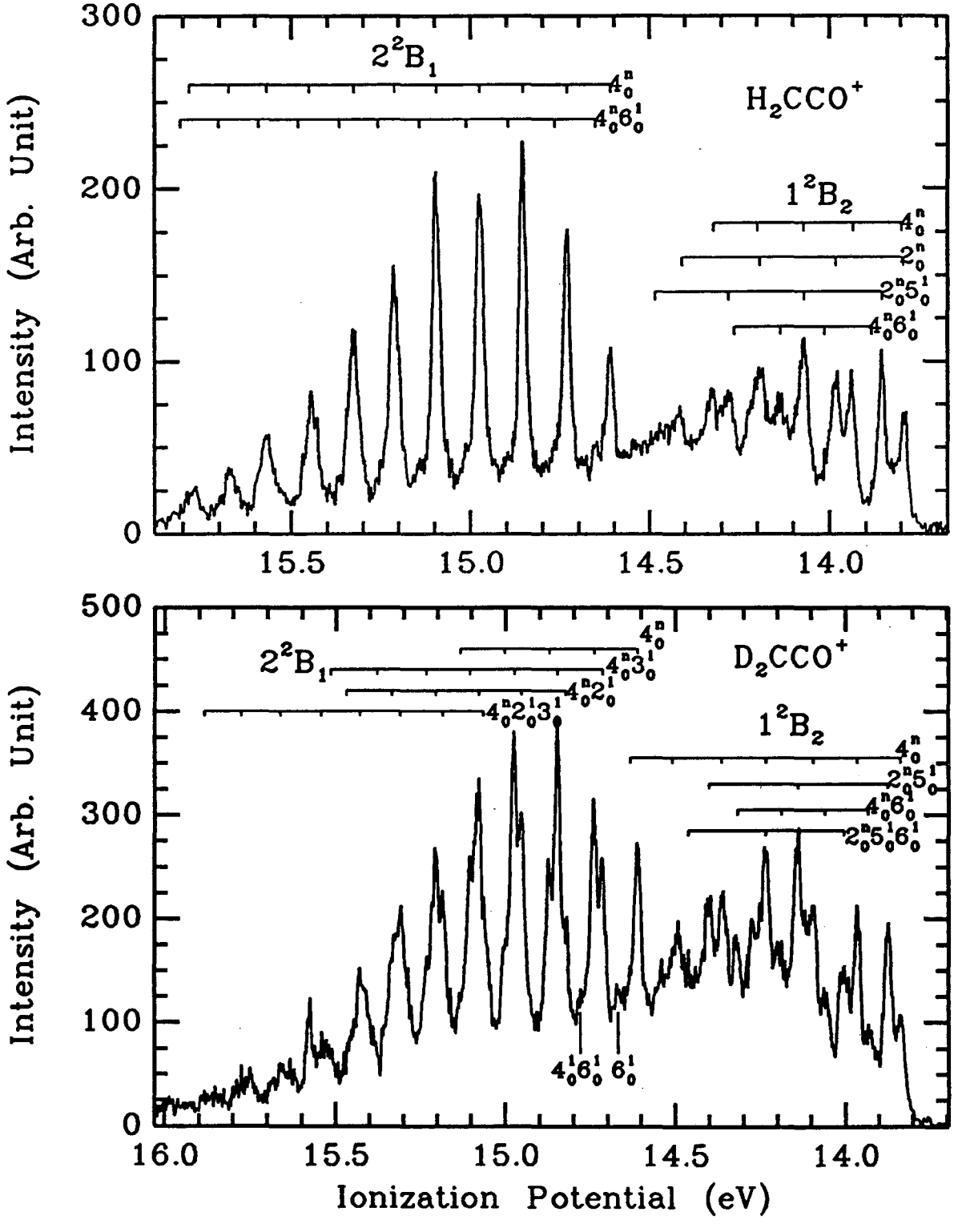
300
200
100
0
Intensity (Arb. Unit)
2^2B_1
4_0^n
$4_0^n6_0^1$
H_2CCO^+
1^2B_2
4_0^n
2_0^n
$2_0^n5_0^1$
$4_0^n6_0^1$
15.5
15.0
14.5
14.0
500
400
300
200
100
0
Intensity (Arb. Unit)
2^2B_1
4_0^n
$4_0^n3_0^1$
$4_0^n2_0^1$
$4_0^n2_0^13^1$
D_2CCO^+
1^2B_2
4_0^n
$2_0^n5_0^1$
$4_0^n6_0^1$
$2_0^n5_0^16_0^1$
$4_0^16_0^1$ 6_0^1
16.0
15.5
15.0
14.5
14.0
Ionization Potential (eV)

Figure 6

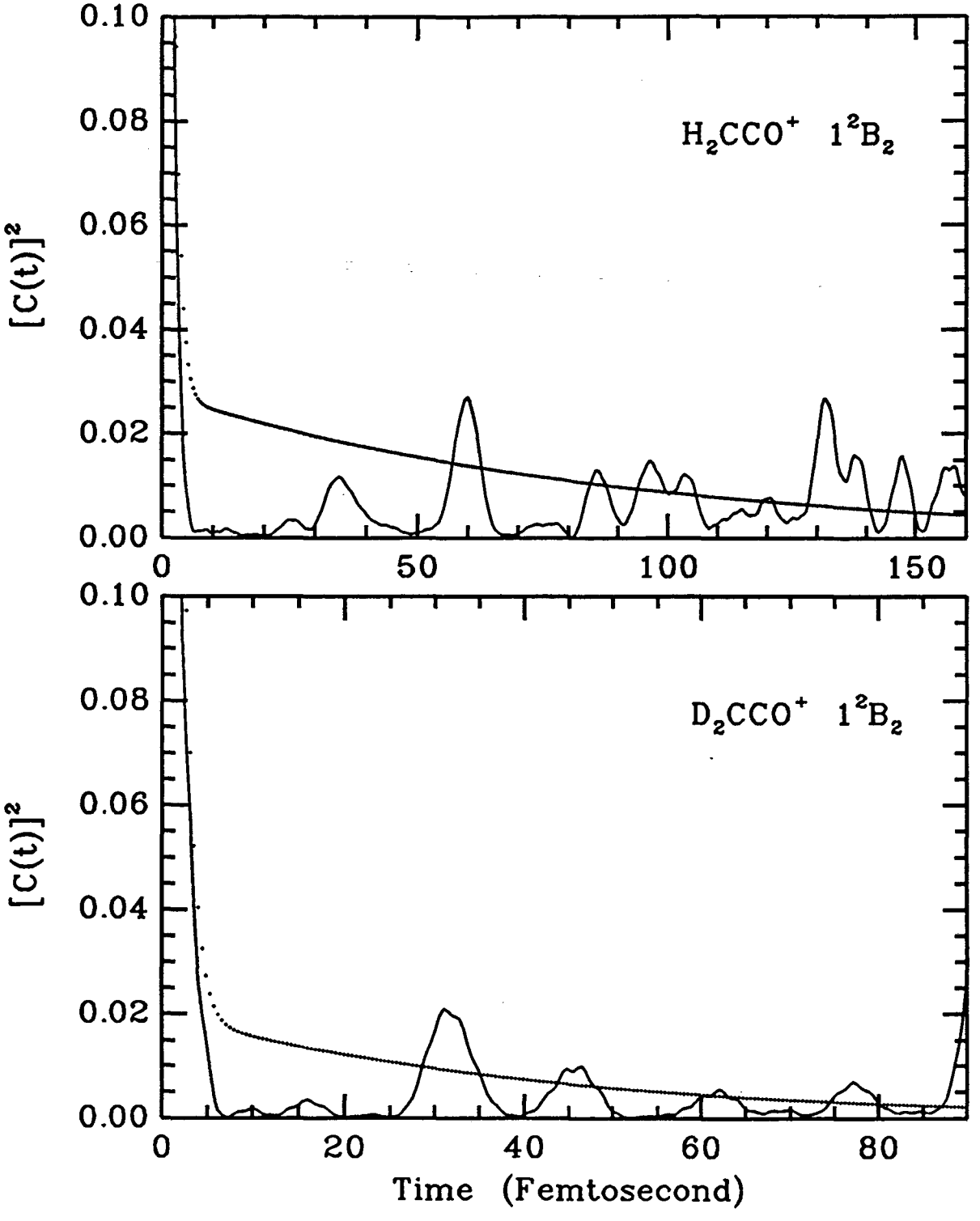
0.10
0.08
0.06
0.04
0.02
0.00
[C(t)]²
H₂CCO⁺ 1²B₂
0
50
100
150
0.10
0.08
0.06
0.04
0.02
0.00
[C(t)]²
D₂CCO⁺ 1²B₂
0
20
40
60
80
Time (Femtosecond)

Figure 7

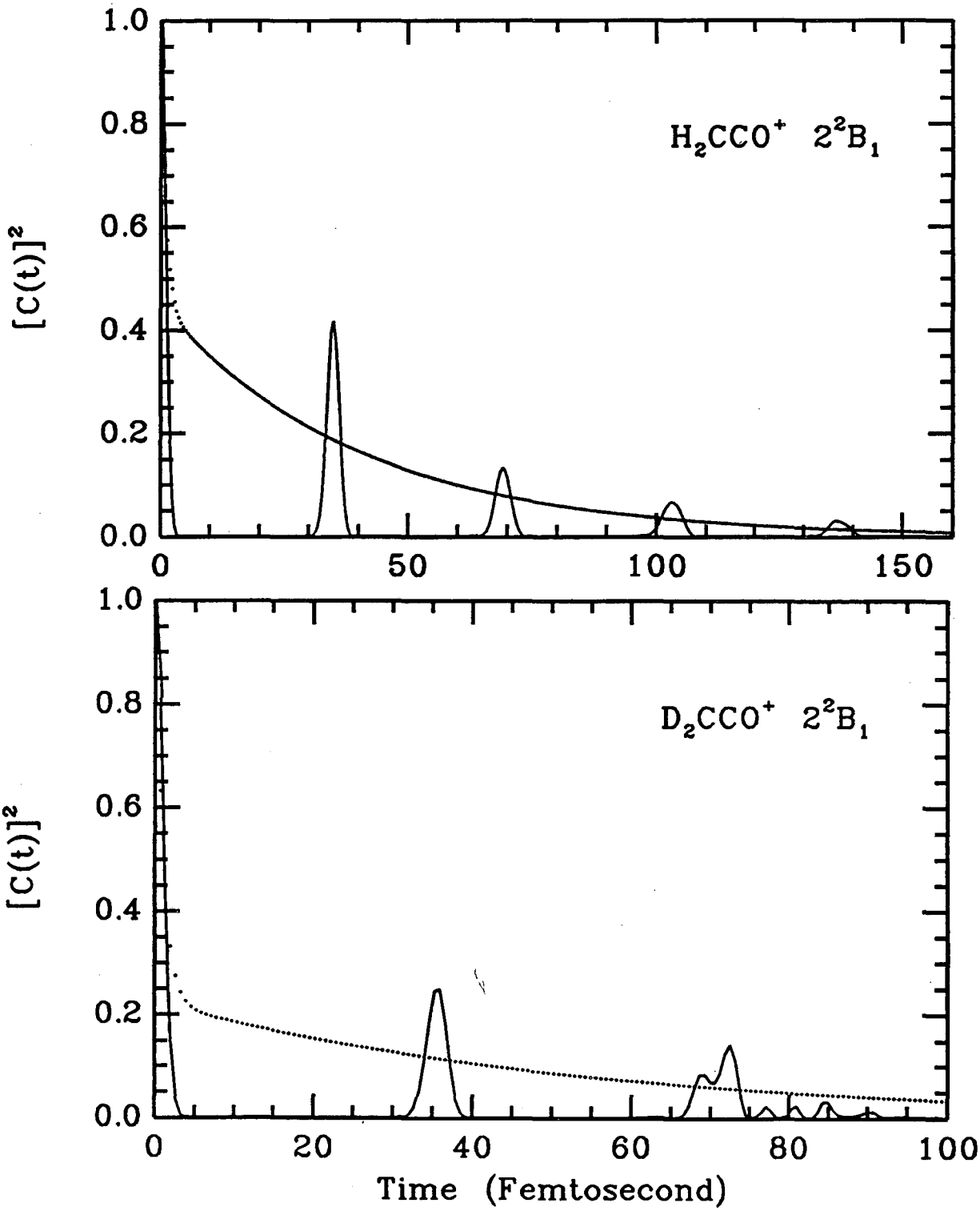
1.0
0.8
0.6
0.4
0.2
0.0
[C(t)]²
H₂CCO⁺ 2²B₁
0
50
100
150
1.0
0.8
0.6
0.4
0.2
0.0
[C(t)]²
D₂CCO⁺ 2²B₁
0
20
40
60
80
100
Time (Femtosecond)

Figure 8.

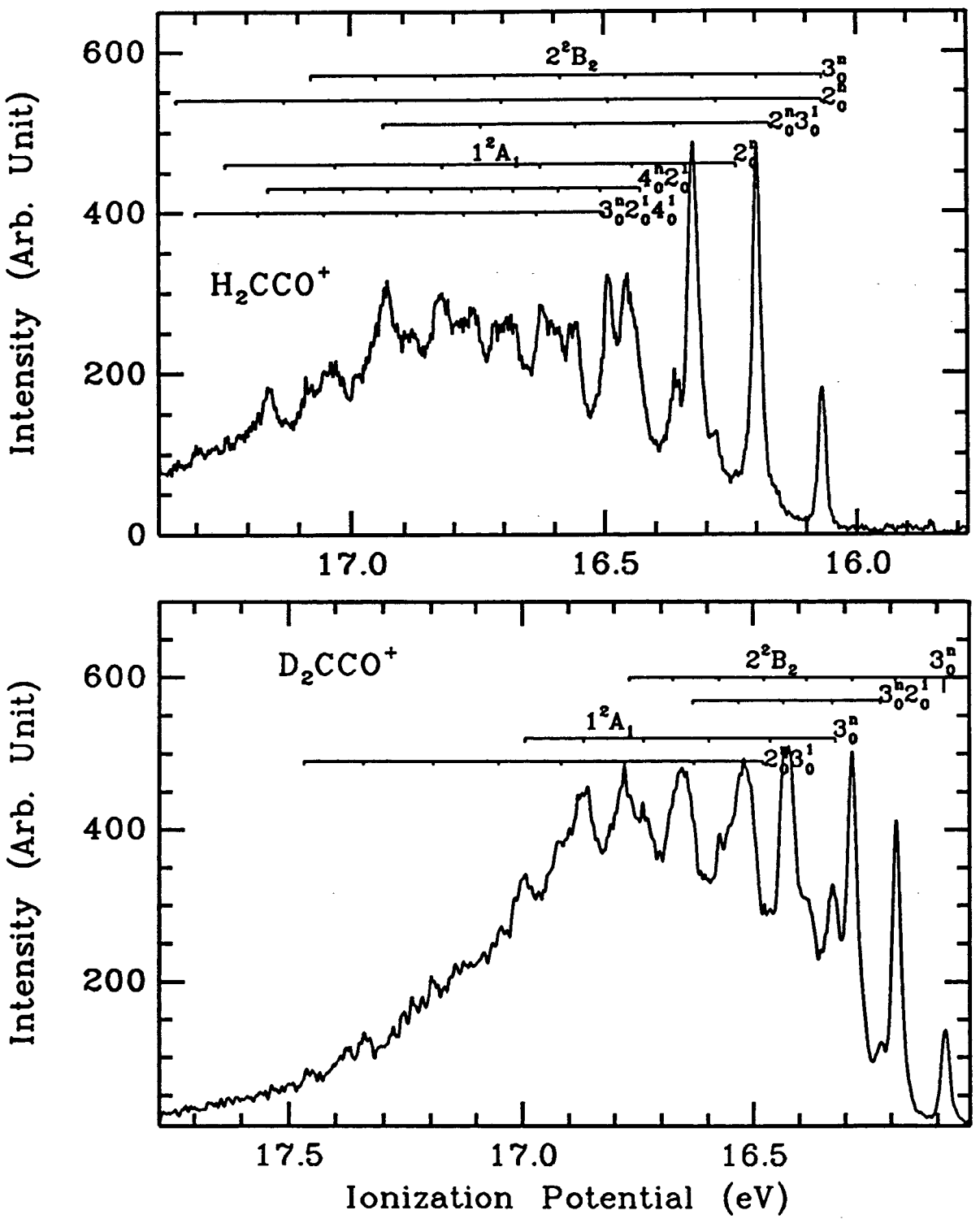
600
400
200
0
Intensity (Arb. Unit)
2^2B_2
3_0^n
2_0^n
$2_0^n3_0^1$
1^2A_1
2_0^n
$4_0^n2_0^1$
$3_0^n2_0^14_0^1$
H_2CCO^+
17.0
16.5
16.0
600
400
200
Intensity (Arb. Unit)
D_2CCO^+
2^2B_2
3_0^n
$3_0^n2_0^1$
1^2A_1
3_0^n
$2_0^n3_0^1$
17.5
17.0
16.5
Ionization Potential (eV)

Figue 9

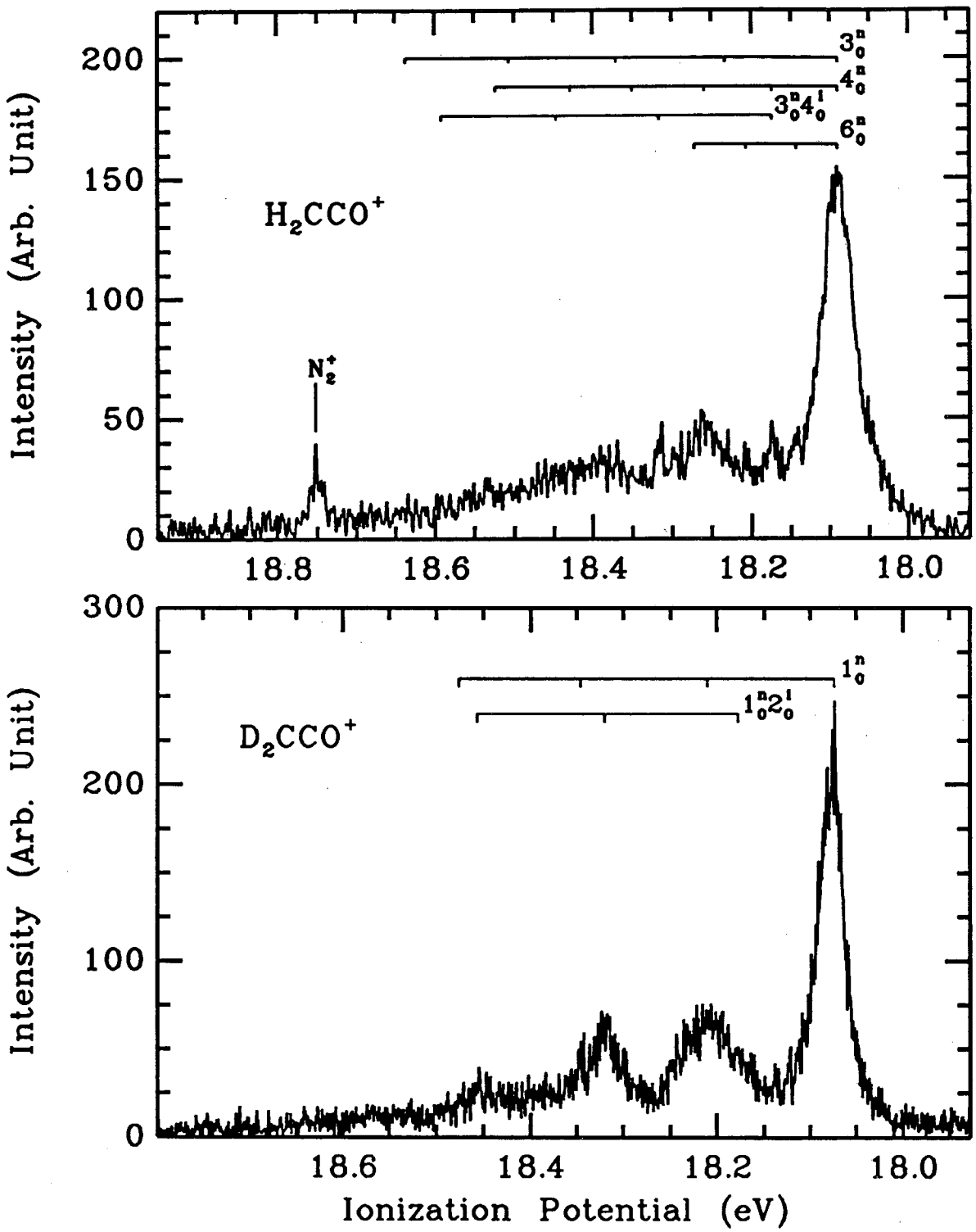
200
150
100
50
0
Intensity (Arb. Unit)
H_2CCO^+
N_2^+
3_0^n
4_0^n
$3_0^n4_0^1$
6_0^n
18.8
18.6
18.4
18.2
18.0
300
200
100
0
Intensity (Arb. Unit)
D_2CCO^+
1_0^n
$1_0^n2_0^1$
18.6
18.4
18.2
18.0
Ionization Potential (eV)

Figure 10

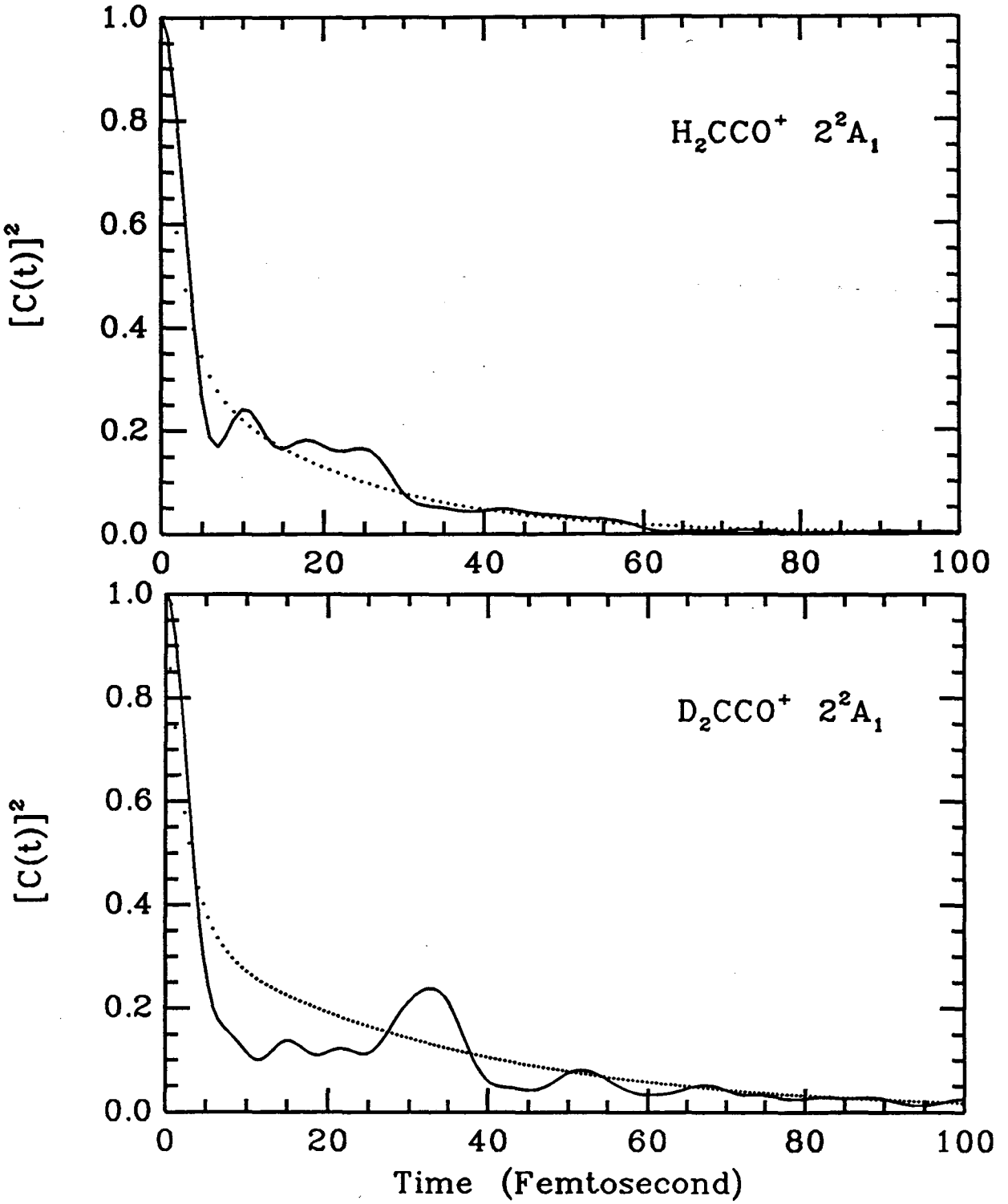
1.0
0.8
0.6
0.4
0.2
0.0
[C(t)]²
H₂CCO⁺ 2²A₁
0
20
40
60
80
100
D₂CCO⁺ 2²A₁
Time (Femtosecond)

Figure 11

LAWRENCE BERKELEY LABORATORY
UNIVERSITY OF CALIFORNIA
TECHNICAL INFORMATION DEPARTMENT
BERKELEY, CALIFORNIA 94720